J Dyn Diff Equat
DOI 10.1007/s10884-013-9339-9

Torus Bifurcations in a Mechanical System

Taoufik Bakri · Yuri A. Kuznetsov · Ferdinand Verhulst

Received: 16 October 2012 / Revised: 16 April 2013

Abstract To study the dynamics and bifurcations of periodic solutions and tori, we consider a self-excited as well as parametrically excited three-mass chain system (a Tondl model) in 1:2:3 resonance. For the analysis both averaging-normalization and numerical simulations are used. First, we consider the case with the upper and lower mass almost equal, but not necessarily in 1:2:3 resonance. Surprisingly, this case simplifies at first order to a system of two coupled oscillators and one uncoupled. A set of necessary and sufficient conditions is then given for the general system to be in 1:2:3 resonance; the conditions can be resolved analytically. Using averaging-normalization, we are able to locate different periodic solutions. A bifurcation diagram is produced for each of the resonances generated by the quasi-periodic solutions, revealing interesting dynamics like a stable 2-torus, torus doubling and in the neighborhood of a Hopf–Hopf bifurcation a stable 3-torus. These tori eventually break up, leading to strange attractors and chaos, in agreement with the Ruelle–Takens (Commun Math Phys 20:167–192, 1971) scenario. Comparing the results of averaging-normalization with the dynamics of the original system shows good agreement. The bifurcation diagram of the normal form shows a complex accumulation of period doublings.

This article is dedicated to the memory of Klaus Kirchgässner, an inspiring mathematician and a good friend.

T. Bakri · Y. A. Kuznetsov · F. Verhulst
Mathematisch Instituut, University of Utrecht,
PO Box 80.010, 3508 TA Utrecht, The Netherlands
e-mail: I.A.Kouznetsov@uu.nl

F. Verhulst
e-mail: F.Verhulst@uu.nl

Present Address:
T. Bakri (✉)
TNO Built Environment and Geosciences,
PO Box 49, 2600 AA Delft, The Netherlands
e-mail: taoufik.bakri@tno.nl

Published online: 26 November 2013

1 Introduction

The bifurcation theory of equilibria is well-developed in the general dissipative setting; see for instance [3,10] or [17]. Especially the generic codimension 1 bifurcations like saddle–node and Hopf have found wide application. A Hopf bifurcation of a periodic solution or a fixed point of a map characterising a dynamical system is usually referred to as Neimark–Sacker bifurcation; such a bifurcation produces a torus around the periodic solution or an invariant circle around a fixed point of its Poincaré map. The flow on the torus is quasi-periodic and may contain isolated periodic solutions. In its turn, such a torus may experience bifurcations of its quasi-periodic flow, resulting in interesting complex dynamics. In a visionary paper by Ruelle and Takens it is argued that an equilibrium can produce a periodic solution by Hopf bifurcation, followed in subsequent bifurcation by a torus. In addition, bifurcations of a torus can produce very complex dynamics. As stated in [21, Sect. 9]: "a quasi-periodic flow on a torus gives flows with strange attractors and more generally, flows which are not Morse-Smale." The quasi-periodic solutions produce an infinite number of resonances, resulting in fractal (Cantor) sets for the bifurcations in parameter space. It was also suggested in [21] (see also [22]) that this route to chaos could be essential for understanding the nature of turbulence; this conjecture is still open.

A number of papers have studied the bifurcations of invariant circles in maps which is the analogue of bifurcations of a 2-torus in a system of differential equations. Early papers in this context are [2,4,25]. Important new directions in the theory can be found in [11,20,31] and [9]. For an extensive bibliography see [10].

Application of these ideas in mechanics are still relatively rare. The case of two coupled oscillators producing torus bifurcations is considered in [6] where evolution to non-smooth tori and 'strange' dynamics is one of the aspects. Related dynamics has also been found and studied in [5,6,19,27,30] and the references therein.

However, in this respect there is not much known about systems of three coupled oscillators involving parametric excitation which corresponds with the analysis of six-dimensional maps. To study such cases, we consider a system of three coupled oscillators that was first proposed by Tondl (2002, Private communication) to model a mechanical device subjected to self-excited vibration. Abadi [1] did a restricted inventory of the equilibria using the averaging method. He also established under which conditions of the involved parameters, the trivial solution is asymptotically stable. The perspective of [1] and (Tondl, 2002, Private communication) corresponded with the engineering wish to suppress 'undesirable' oscillations by stabilising the trivial solution. However, we are interested in more or less the opposite questions i.e. we will investigate these 'undesirable' oscillations and study their bifurcations; it turns out that in this higher-dimensional setting, we will find new phenomena.

The analysis can be carried out by averaging-normalization [23] and numerical bifurcation techniques developed and contained in AUTO [8,15], CONTENT [18] and MATCONT [26].

The engineering context is as follows. Consider the three-mass system as sketched in Fig. 1. The mass m_2 is self-excited by flow, which is modeled by a Rayleigh term. The masses m_1 and m_3 are coupled to m_2 and can be parametrically excited. If one wishes to quench the motion of the self-excited mass m_2, with a suitable tuning, the masses m_1 and m_2 can be used as energy absorbers. The equations of motion are as follows:

$$\begin{cases} m_1\ddot{y}_1 + b\dot{y}_1 + k_0(1+\varepsilon\cos\omega t)y_1 - k_1(y_2 - y_1) = 0, \\ m_2\ddot{y}_2 - \beta_0 U^2(1-\gamma_0\dot{y}_2^2)\dot{y}_2 + 2k_1 y_2 - k_1(y_1 + y_3) = 0, \\ m_3\ddot{y}_3 + b\dot{y}_3 + k_0(1+\varepsilon\cos\omega t)y_3 - k_1(y_2 - y_3) = 0. \end{cases} \tag{1}$$

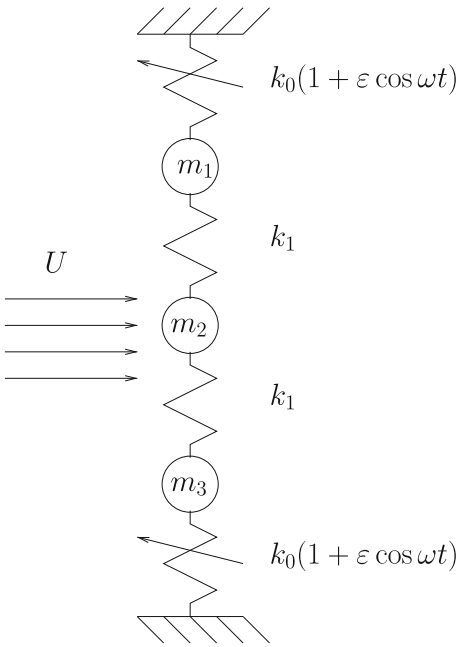

Fig. 1 The three-mass system under consideration

Here y_1, y_2 and y_3 represent the deflections of the masses m_1, m_2 and m_3 respectively. The parameters k_0, k_1, γ_0 are assumed to be positive. The parameter ε is assumed to be small and positive. The Rayleigh excitation parameter β_0 and the damping coefficient b are assumed to be $O(\varepsilon)$, $b = \varepsilon\bar{\kappa}$ and $\beta_0 = \varepsilon\bar{\beta}$, whereas all the remaining parameters are constants which do not depend on ε.

In this study we shall distinguish between two cases, the relatively simple symmetric case $m_1 = m_3$, which will be discussed for general mass ratio m_1/m_2 in Sect. 2, and the case $m_1 \neq m_3$. The dynamics of these two cases turn out to be very different from each other. From Sect. 3 on, we choose $m_1 \neq m_3$ and as an interesting case the internal 1:2:3 resonance because this case is one of the first-order resonances to study (the notion of internal resonance applies to the ratio of the basic frequencies of the three coupled oscillators where certain perturbations are omitted). The basic frequencies if $\varepsilon = 0$ are ω_0, $2\omega_0$, $3\omega_0$. After obtaining the variational equations for the internal 1:2:3 resonance, the $O(\varepsilon)$ terms contain parametric excitations that can be in resonance with the basic oscillations (frequencies $n\omega_0$, $n = 1, 2, 3$); there are nine possibilities. From Sect. 4 on, we consider the case $n = 1$. The other eight parametric resonances are still open problems.

Apart from many codimension one and codimension two standard bifurcations, we will find very complex dynamics involving 2-tori, 3-tori, torus doubling and a route to chaos.

2 The Almost-Symmetric Case $m_3 = (1 + \varepsilon\rho)m_1$

Let's start by considering the first case i.e. $m_3 = (1 + \varepsilon\rho)m_1$, with $0 \leq \varepsilon \ll 1$ and ρ a parameter that does not depend on ε. Consider system (1) with this choice of m_3 and apply the transformation $\tau = \omega_0 t$ with $\omega_0 = \sqrt{2k_1/m_2}$; we find with some rearrangements the following system:

$$\begin{cases} y_1'' + q^2 y_1 - \frac{M}{2}(y_2 - y_1) = -\varepsilon(\bar{\kappa} y_1' + q^2 y_1 \cos \eta\tau), \\ y_2'' + y_2 - \frac{1}{2}(y_1 + y_3) = \varepsilon\bar{\beta} V^2 (1 - \gamma y_2'^2) y_2', \\ y_3'' + q^2 y_3 - \frac{M}{2}(y_2 - y_3) = -\varepsilon\left(\bar{\kappa} y_3' + q^2 y_3 \cos \eta\tau - \rho\left(q^2 + \frac{M}{2}\right) y_3 + \rho \frac{M}{2} y_2\right) + O(\varepsilon^2). \end{cases} \tag{2}$$

In the above $M = \frac{m_2}{m_1}$, $\kappa = \frac{b}{m_1\omega_0}$, $\kappa = \varepsilon\bar{\kappa}$, $q^2 = \frac{k_0}{m_1\omega_0^2}$, $\gamma = \omega_0^2\gamma_0$, $\beta = \frac{\beta_0 U_0^2}{m_2\omega_0}$, $\beta = \varepsilon\bar{\beta}$, $\eta = \frac{\omega}{\omega_0}$, $V = \frac{U}{U_0}$ and U_0 is a chosen reference value for the flow velocity. System (2) can be written in the vector form:

$$Y'' = AY + \varepsilon F(Y', Y, \tau),$$

with

$$A = \begin{pmatrix} -\left(q^2 + \frac{M}{2}\right) & \frac{M}{2} & 0 \\ \frac{1}{2} & -1 & \frac{1}{2} \\ 0 & \frac{M}{2} & -\left(q^2 + \frac{M}{2}\right). \end{pmatrix}$$

In what follows we transform the system into quasi-normal form by a coordinate transformation. Using this new form, we can see from the eigenvalues of A which basic resonances the system can possibly take. How this is done is briefly sketched below. The eigenvalues of the matrix A are:

$$\begin{aligned} \lambda_1 &= \alpha, \\ \lambda_2 &= \frac{1}{2}\left(\alpha - 1 - \sqrt{(\alpha - 1)^2 - 4q^2}\right), \\ \lambda_3 &= \frac{1}{2}\left(\alpha - 1 + \sqrt{(\alpha - 1)^2 - 4q^2}\right), \end{aligned} \tag{3}$$

with

$$\alpha = -\left(q^2 + \frac{M}{2}\right). \tag{4}$$

Remark One can easily check that $\lambda_1 \neq \lambda_2 \neq \lambda_3$ for all the values of the parameters in the parameter space under consideration. This guarantees the diagonalisation of the matrix A. The corresponding eigenvector matrix is:

$$C = \begin{pmatrix} -1 & 1 & 1 \\ 0 & d & e \\ 1 & 1 & 1 \end{pmatrix}, \quad \text{with inverse matrix } C^{-1} = \begin{pmatrix} -\frac{1}{2} & 0 & \frac{1}{2} \\ d' & e' & d' \\ d' & -e' & d' \end{pmatrix}.$$

The parameters d' and e' are related to the parameters d and e which can be computed easily by determining the eigenvectors of the matrix A. How exactly e' and d' are related to e and d is not important at this stage. Applying the transformation $Y = CX$ yields the following system of equations in X which is now in quasi-normal form.

$$x_i'' + \omega_i^2 x_i = \varepsilon\langle C^{-1}(F(CX', CX, \tau)), e_i\rangle, \quad i = 1, 2, 3 \text{ and } \omega_i^2 = -\lambda_i. \tag{5}$$

Where $\langle . \, , \, . \rangle$ denotes the standard inner product in $\mathbb{R}^3$.

Proposition 1 *System (5) will always decouple after first-order averaging no matter what the involved parameters and resonances are.*

Proof To see this, we will show that the first equation decouples from the other two. Let's write down explicitly the first equation of system (5). We shall in what follow omit the bars for notational simplicity. We get the following equation:

$$x_1'' + \omega_1^2 x_1 = \frac{\varepsilon}{2}\left[-2\kappa x_1' + 2q^2 x_1 \cos\eta\tau + \rho\left(q^2 + \frac{M}{2}\right)x_1 + \rho\left(q^2 - \frac{M}{2}(d-1)\right)x_2 + \rho\left(q^2 - \frac{M}{2}(e-1)\right)x_3\right] + O\left(\varepsilon^2\right). \tag{6}$$

One can easily check that

$$\omega_1^2 = q^2 + \frac{M}{2},\ \omega_2^2 = q^2 - \frac{M}{2}(d-1),\ \text{and}\ \omega_3^2 = q^2 - \frac{M}{2}(e-1).$$

The first equation reduces then to the following:

$$x_1'' + \omega_1^2 x_1 = \frac{\varepsilon}{2}\left[-2\kappa x_1' + 2q^2 x_1 \cos\eta\tau + \rho\omega_1^2 x_1 + \rho\omega_2^2 x_2 + \rho\omega_3^2 x_3\right] + O(\varepsilon^2). \tag{7}$$

Introducing the phase amplitude coördinates, $x_i = R_i\cos(\omega_i\tau + \phi_i)$, and omitting the $O(\varepsilon^2)$ terms, we get the following equation for R_1' and ϕ_1'.

$$\begin{aligned}
R_1' =& \frac{\varepsilon}{4\omega_1}\Big[\Big(-2\kappa\omega_1 + 2\kappa\omega_1\cos(2\phi_1 + 2\omega_1\tau)\rho\omega_1^2\sin(2\phi_1 + 2\omega_1\tau) \\
&- q^2\sin(2\phi_1 - \eta\tau + 2\omega_1\tau) - q^2\sin(2\phi_1 + \eta\tau + 2\omega_1\tau)\Big)R_1 \\
&- \Big(\sin(\phi_1 - \phi_2 + (\omega_1 - \omega_2)\tau) + \sin(\phi_1 + \phi_2 + (\omega_1 + \omega_2)\tau)\Big)\rho\omega_2^2 R_2 \\
&- \Big(\sin(\phi_1 - \phi_3 + (\omega_1 - \omega_3)\tau) + \sin(\phi_1 + \phi_3 + (\omega_1 + \omega_3)\tau)\Big)\rho\omega_3^2 R_3\Big]. \\
\phi_1' =& \frac{\varepsilon}{4\omega_1 R_1}\Big[\Big(-\rho\omega_1^2 - q^2\cos\eta\tau - \rho\omega_1^2\cos(2\phi_1 + 2\omega_1\tau) \\
&- q^2\cos(2\phi_1 - \eta\tau + 2\omega_1\tau) - q^2\cos(2\phi_1 + \eta\tau + 2\omega_1\tau)\Big)R_1 \\
&- \Big(\cos(\phi_1 - \phi_2 + (\omega_1 - \omega_2)\tau) + \cos(\phi_1 + \phi_2 + (\omega_1 + \omega_2)\tau)\Big)\rho\omega_2^2 R_2 \\
&- \Big(\cos(\phi_1 - \phi_3 + (\omega_1 - \omega_3)\tau) + \cos(\phi_1 + \phi_3 + (\omega_1 + \omega_3)\tau)\Big)\rho\omega_3^2 R_3\Big].
\end{aligned}$$

One observes in the expressions for R_1' and ϕ_1' that the averaged system will couple if and only if $\omega_1 = \omega_2$ or $\omega_1 = \omega_3$. This means $\lambda_1 = \lambda_2$ or $\lambda_1 = \lambda_3$. Combining this with equation (3) we get the following equation for α:

$$\alpha + 1 = \pm\sqrt{(\alpha - 1)^2 - 4q^2}.$$

It follows that M must be equal to zero which is equivalent to the case $m_2 = 0$. This is however excluded in our study otherwise we would only have a system of two coupled oscillators. This concludes the proof. □

2.1 Conclusion

The case $m_3 \simeq m_1$ always reduces, after averaging, to a system of two coupled oscillators and one completely decoupled. In other words, the symmetric case implies a remarkable simplification. This does not mean however that one of the masses oscillates completely independently of the other two. Note that a coordinates transformation has been made before putting the mechanical system in quasi-normal form so that we no longer can relate (without transformation) the new coordinates to a single mass.

System (2) is interesting from a dynamical systems point of view, but as we will focus in this paper on phenomena in a three degrees-of-freedom context, we will not continue with this case.

3 The Case $m_1 \neq m_3$ in 1:2:3 Internal Resonance

In this case the system does not necessarily decouple as we shall see later on. We focus in what follows on the 1:2:3 resonance case in system (1). The other primary resonances are 1:2:1, 1:2:2 and 1:2:4; these resonances merit separate papers.

One can assume without loss of generality $k_0 = 1$ and $m_1 = 1$. With $\lambda = 1/m_2$ and $\mu = 1/m_3$, system (1) can be transformed, after some rescaling, into the following system.

$$\begin{cases} y_1'' + \left(\frac{1}{k_1} + 1\right) y_1 - y_2 = -\varepsilon \left[\frac{b}{\sqrt{k_1}} y_1' + \frac{1}{k_1} \cos \frac{\omega\tau}{\sqrt{k_1}}\ y_1\right], \\ y_2'' - \lambda y_1 + 2\lambda y_2 - \lambda y_3 = \frac{\varepsilon\lambda\beta_0 U^2}{\sqrt{k_1}} (1 - \gamma_0 k_1 y_2'^2) y_2', \\ y_3'' - \mu y_2 + \mu \left(\frac{1}{k_1} + 1\right) y_3 = -\varepsilon \left[\frac{b\mu}{\sqrt{k_1}} y_3' + \frac{\mu}{k_1} \cos \frac{\omega\tau}{\sqrt{k_1}}\ y_3\right]. \end{cases} \tag{8}$$

3.1 Conditions for the System to be in 1:2:3 Resonance

When a system like (1) or (8) is in 1:2:3 resonance, its frequencies will be $\omega_0,\ 2\omega_0,$ and $3\omega_0$. We shall in what follows refer to ω_0 as the 'basic frequency of the system'. With the parameter k_1 given, to force the system into the 1:2:3 resonance, the parameters μ, λ must satisfy the following system of equations:

$$\begin{cases} -a\mu - 2\lambda = 14\theta + a, \\ -a^2\mu - (2a-1)\lambda - (2a-1)\lambda\mu = -49\theta^2, \\ 2a(1-a)\lambda\mu = 36\theta^3, \end{cases} \tag{9}$$

where $\theta = -\omega_0^2$ and $a = (1/k_1 + 1)$.

Remark on symmetry System (9) has a hidden symmetry: if (μ, λ, θ) is a solution, then so is $(\mu^{-1}, \lambda\mu^{-1}, \theta\mu^{-1})$. Solving system (9) for the mass ratios μ and λ yields

$$\begin{cases} \mu = (2a-1) + \frac{14}{a}(2a-1)\theta + \frac{98}{a}\theta^2 + \frac{36(2a-1)}{a^2(a-1)}\theta^3, \\ \lambda = -a^2 - 14a\theta - 49\theta^2 - \frac{18(2a-1)}{a(a-1)}\theta^3, \end{cases} \tag{10}$$

where θ is a root of the following sixth degree algebraic polynomial

$$\begin{aligned} P(x) = {} & 648(1-2a)^2x^6 + 3528a(1-3a+2a^2)x^5 + 14a(-18+469a \\ & -938a^2+487a^3)x^4 - 2a^2(343-2112a+3213a^2-1444a^3)x^3 \\ & +49a^3(1-a)^2(12a-5)x^2 + 28a^4(a-1)^2(2a-1)x \\ & +a^5(a-1)^2(2a-1). \end{aligned} \tag{11}$$

From this polynomial we see that the 1:2:3 resonance occurs at most at six different places in (μ, λ)-parameter space.

Example $a = 2$

In this case the polynomial $P(x)$ is irreducible. We therefore compute numerically its roots. There are two real roots. Namely, $\theta_1 \simeq -.250224$ and $\theta_2 \simeq -0.641144$. Using equation (10), these two values of θ yield $\mu_1 \simeq 0.390277$, $\mu_2 \simeq 2.56228$, $\lambda_1 \simeq 0.36129$ and $\lambda_2 \simeq 0.925727$.

Remark One can easily check that $\mu_2 = \mu_1^{-1}$, $\lambda_2 = \lambda_1\mu_1^{-1}$ and $\theta_2 = \theta_1\mu_1^{-1}$.

Remark Using the hidden symmetry mentioned above we were able to produce the following factorisation of the polynomial $P(x)$ in the case $a = 2$.

$$\begin{aligned} P(x) = {} & -\frac{8}{243}\left(-21+3\sqrt[3]{19}+\left(-98+7\sqrt[3]{19}+\sqrt[3]{19^2}\right)x-81x^2\right) \\ & \times\left(147+21\sqrt[3]{19}+3\sqrt[3]{19^2}+\left(1353+147\sqrt[3]{19}+21\sqrt[3]{19^2}\right)x\right. \\ & +\left(4291+316\sqrt[3]{19}+49\sqrt[3]{19^2}\right)x^2 \\ & \left.+\left(5292+189\sqrt[3]{19}+27\sqrt[3]{19^2}\right)x^3+2187x^4\right). \end{aligned} \tag{12}$$

From this expression we can exactly compute the roots of the polynomial $P(x)$. We find two real roots:

$$\theta_1 = \frac{1}{162}\left(-98+7\sqrt[3]{19}+\sqrt[3]{19^2}+\sqrt{3066-381\sqrt[3]{19}-147\sqrt[3]{19^2}}\right), \tag{13}$$

$$\theta_2 = \frac{1}{162}\left(-98+7\sqrt[3]{19}+\sqrt[3]{19^2}-\sqrt{3066-381\sqrt[3]{19}-147\sqrt[3]{19^2}}\right). \tag{14}$$

From these explicit formula's for θ, and using Eq. (10), one gets exact formula's for the mass ratios μ and λ to produce the 1:2:3 resonance.

Example $a = 3$

$P(x)$ is reducible and has six real roots which can be computed in radicals. We give here the roots in five decimals.

$\theta_1 = -2.21525$, $\theta_2 = -0.451416$, $\theta_3 = -2.22248$, $\theta_4 = -0.826402$, $\theta_5 = -0.470972$, and $\theta_6 = -0.346815$.

From these explicit formula's for θ, and using Eq. (10), one gets exact formula's for the mass ratios μ and λ needed to be on the 1:2:3 resonance. We see that there are in this case six

different places in the $(\mu, \lambda)-$parameter space where the 1:2:3 resonance occur. We find the following values for μ and λ

$$\begin{aligned} \mu_1 &= 4.90735, & \mu_3 &= 4.71887, & \mu_4 &= 2.38284, \\ \lambda_1 &= 6.64573, & \lambda_3 &= 6.97905, & \lambda_4 &= 0.710559. \end{aligned}$$

The remaining values of μ and λ can be obtained from these values using the symmetry.

3.2 The Basic Frequency ω_0 and the Mass Ratio as a Tends to Infinity

One can continue the roots of the polynomial $P(x)$ with respect to the parameter a. Starting at the point $\theta = \theta_1$ and $a = 2$ we found that the roots collapse and disappear in a fold (saddle–node) bifurcation; (LP) in Figs. 2 and 3 indicates a fold bifurcation as the parameter a decreases. For increasing values of the parameter a, the frequencies become almost linear

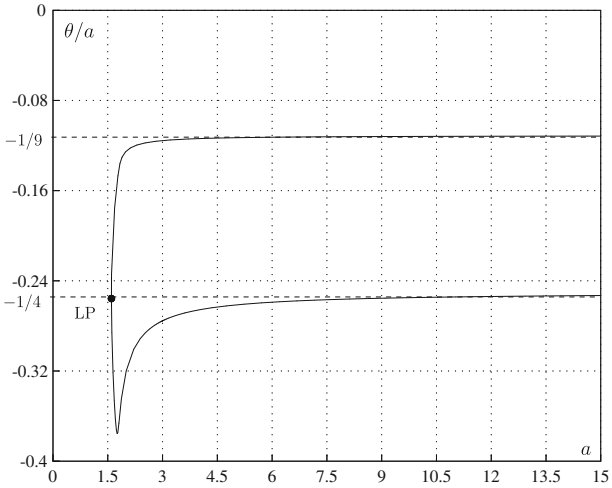

Fig. 2 The behaviour of the frequency $\theta = -\omega_0^2$ as a tends to infinity

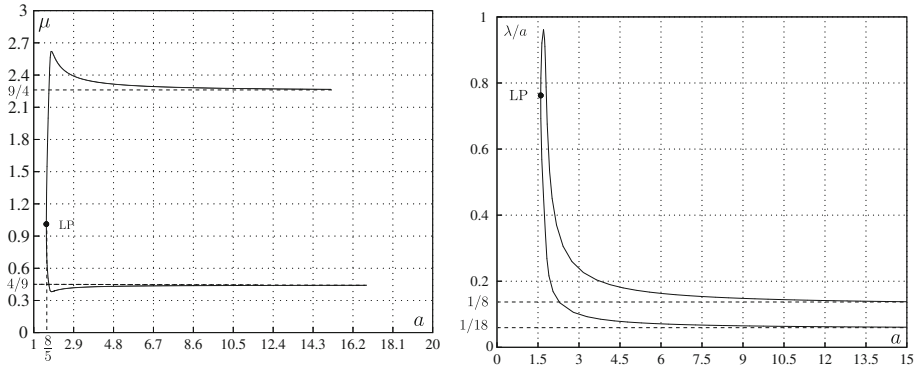

Fig. 3 The behaviour of the mass ratio μ and the ratio λ/a as a tends to infinity; *LP* indicates a fold (saddle–node) bifurcation

proportional to the parameter a. The graph of the mass ratio μ as a function of the parameter a has two horizontal asymptotes. See Figs. 2 and 3, generated by CONTENT [18], below.

This looks peculiar; however the explanation for this limiting behaviour is that the polynomial $P(x)$ can be written as follows:

$$P(x) = a^8 Q_a\left(\frac{x}{a}\right), \tag{15}$$

with

$$\begin{aligned} Q_a(x) = &\left(-2 + \frac{1}{a^3} - \frac{4}{a^2} + \frac{5}{a}\right) + \left(\frac{28}{a^3} - \frac{112}{a^2} + \frac{140}{a} - 56\right) x \\ &+ \left(\frac{245}{a^3} - \frac{1078}{a^2} + \frac{1421}{a} - 588\right) x^2 \\ &+ \left(\frac{686}{a^3} - \frac{4224}{a^2} + \frac{6426}{a} - 2888\right) x^3 \\ &+ \left(\frac{252}{a^3} - \frac{6566}{a^2} + \frac{13132}{a} - 6818\right) x^4 \\ &+ \left(-\frac{3528}{a^2} + \frac{10584}{a} - 7056\right) x^5 + \left(-\frac{648}{a^2} + \frac{2592}{a} - 2592\right) x^6. \end{aligned}$$

Note that $P(x) = 0$, if and only if $Q_a\left(\frac{x}{a}\right) = 0$. As the parameter a tends to infinity the polynomial $Q_a(x)$ tends to the following:

$$Q_\infty(x) = -2(1+x)^2(1+4x)^2(1+9x)^2.$$

This polynomial has three double roots. This means $\lim_{a\to\infty}\left(\frac{\theta}{a}\right) = l$, with $l \in \{-1, -\frac{1}{4}, -\frac{1}{9}\}$. It explains the almost linear behaviour of θ with respect to the parameter a, for high values of a shown in Fig. 2 above. Solving system (10) for a tending to infinity yields the following possible solutions for the 1:2:3 resonance.

$$\begin{aligned} &(\tilde{\theta}_1, \mu_1, \tilde{\lambda}_1) = (-1, 4, 9/2), \ (\tilde{\theta}_2, \mu_2, \tilde{\lambda}_2) = (-1, 9, 2), \\ &(\tilde{\theta}_3, \mu_3, \tilde{\lambda}_3) = (-1/4, 1/4, 9/8), (\tilde{\theta}_4, \mu_4, \tilde{\lambda}_4) = (-1/4, 9/4, 1/8), \\ &(\tilde{\theta}_5, \mu_5, \tilde{\lambda}_5) = (-1/9, 1/9, 2/9), \text{ and } (\tilde{\theta}_6, \mu_6, \tilde{\lambda}_6) = (-1/9, 4/9, 1/18). \end{aligned}$$

With

$$\tilde{\lambda}_i = \frac{\lambda_i}{a}, \text{ and } \tilde{\theta}_i = \frac{\theta_i}{a}.$$

Note that the symmetry is not lost in the limiting system.

3.3 Conclusion

To remain in 1:2:3 resonance while the parameter k_1 tends to zero (i.e. the mass m_2 tends to be a free particle), the mass ratios μ, $\tilde{\theta}$ and $\tilde{\lambda}$ have the six possibilities described above.

Remark All the possible numerical values to which the parameter μ tends as a goes to infinity are exactly known. We have in the case $a = 2$ in Fig. 3, $\mu_\infty = \mu_6 = 4/9$ and $\mu_\infty = \mu_4 = 9/4$. The point where the fold bifurcation takes place can also be computed exactly. One finds that the two roots collide and disappear at the critical value $a_c = 8/5$, $\lambda_c = 6/5$, and $\theta_c = -2/5$. This follows from the fact that at the fold point we have $\mu = 1$ which is understandable because the symmetry relation becomes the identity.

3.4 The Almost-Harmonic System

Now that it is exactly known when and under what conditions the system is in 1:2:3 resonance, we can proceed with the study of the normal form and the involved bifurcations in this resonance. Following [1], we will first focus on the relatively easy case $k_1 = 1$, after this we will study the case $k_1 \neq 1$. Using the method sketched in the previous section, it can be shown that system (8) can be transformed into almost-harmonic form (in engineering called quasi-normal form). We find:

$$C = \begin{pmatrix} a_{11} & a_{21} & a_{31} \\ 1 & 1 & 1 \\ a_{12} & a_{22} & a_{32} \end{pmatrix}, \tag{16}$$

with $a_{ij},\ i = 1, 2, 3,\ j = 1, 2$ all nonzero and depending uniquely on the parameters k_1, λ and μ. This produces the almost-harmonic system:

$$\begin{cases} x_i'' + (i\omega_0)^2 x_i = \varepsilon \langle C^{-1}(F(X)), e_i \rangle,\ i = 1, 2, 3 \text{ and } \omega_0^2 = -\theta, \\ F(X) = \left[-\frac{S_1(X)\cos\tilde{\omega}t}{k_1} - \frac{bS_1'(X)}{\sqrt{k_1}}, \frac{\beta_0 \lambda U^2 S_2'(X)(1-\gamma_0 k_1 S_2'(X)^2)}{\sqrt{k_1}}, -\frac{\mu S_3(X)\cos\tilde{\omega}t}{k_1} - \frac{\mu b S_3'(X)}{\sqrt{k_1}} \right]^T, \\ S_1(X) = a_{11}x_1 + a_{21}x_2 + a_{31}x_3,\ S_2(X) = x_1 + x_2 + x_3, \\ S_3(X) = a_{12}x_1 + a_{22}x_2 + a_{32}x_3,\ X = [x_1, x_2, x_3]^T \text{ and } \tilde{\omega} = \omega/\sqrt{k_1}. \end{cases}$$

Written down explicitly in the new variables x_i, with $i = 1, 2, 3$, the quasi-normal form becomes:

$$\begin{aligned} x_i'' + (i\omega_0)^2 x_i = \varepsilon \big(& \theta_{i1}x_1' + \theta_{i2}x_2' + \theta_{i3}x_3' + (Q_{i1}x_1 + Q_{i2}x_2 \\ & + Q_{i3}x_3)\cos(\tilde{\omega}t) + B_i(x_1' + x_2' + x_3')^3 \big), \end{aligned} \tag{17}$$

with,

$$\Theta = (\theta_{ij}) = \frac{1}{\sqrt{k_1}} C^{-1} \begin{pmatrix} -ba_{11} & -ba_{21} & -ba_{31} \\ \beta_0 \lambda U^2 & \beta_0 \lambda U^2 & \beta_0 \lambda U^2 \\ -a_{12}\mu b & -a_{22}\mu b & -a_{32}\mu b \end{pmatrix},$$

$$Q = (Q_{ij}) = \frac{1}{k_1} C^{-1} \begin{pmatrix} -a_{11} & -a_{21} & -a_{31} \\ 0 & 0 & 0 \\ -\mu a_{12} & -\mu a_{22} & -\mu a_{32} \end{pmatrix}, \quad \text{and}$$

$$B = [B_1, B_2, B_3]^T = -\beta_0 \lambda U_0^2 \gamma_0 \sqrt{k_1} C^{-1} e_2.$$

Based on averaging-normalization in the case of system (1), we have to first order the following possibilities for parametric excitation of the internal 1:2:3 resonance: $\omega = n\sqrt{k_1}\omega_0, n = 1, \ldots, 9$.

We shall now proceed with the study of one of the nine different cases, $\omega = \sqrt{k_1}\omega_0$. The other eight cases are still open for investigation. We have seen in the case $k_1 = 1$, that there are two possibilities for the system parameters to produce 1:2:3 resonance. In each case, these possibilities will be investigated. To keep the study concise, we will be interested only in the isolated nontrivial equilibria of the averaged system and their bifurcations. These equilibria correspond in the original system with periodic solutions. The bifurcations of the periodic

solutions may lead to tori, their break-up and eventually to chaos. To study this we introduce the phase-amplitude coordinates:

$$x_i = R_i \cos(i w_0 t + \phi_i), \quad i = 1, \ldots, 3.$$

4 The Parametric Excitation Case $\omega = \sqrt{k_1}\omega_0$

Assume $k_1 = 1$, $\lambda = 0.36129$, $\mu = 0.390277$, $\tilde{\omega} = \omega_0 = 0.500224$. After applying the time transformation $\tilde{\omega}t \to \tilde{t}$ (with appropriate scaling of the coefficients B_i, θ_{ij}, and Q_{ij}), and omitting the tildes for notational simplicity, the averaged system becomes:

$$\begin{aligned}
R_1' &= \frac{1}{8}\varepsilon \left(3B_1R_1^3 + 24B_1R_2^2R_1 + 54B_1R_3^2R_1 + 4\theta_{11}R_1\right.\\
&\quad - 9B_1R_1^2R_3\cos(3\phi_1 - \phi_3) + 36B_1R_2^2R_3\cos(\phi_1 - 2\phi_2 + \phi_3)\\
&\quad \left. - 2Q_{12}R_2\sin(\phi_1 - \phi_2)\right),\\
R_2' &= \frac{1}{8}\varepsilon \left(12B_2R_2^3 + 6B_2R_1^2R_2 + 54B_2R_3^2R_2 + 4\theta_{22}R_2\right.\\
&\quad + 18B_2R_1R_3\cos(\phi_1 - 2\phi_2 + \phi_3)R_2 + Q_{21}R_1\sin(\phi_1 - \phi_2)\\
&\quad \left. - Q_{23}R_3\sin(\phi_2 - \phi_3)\right),\\
R_3' &= -\frac{1}{24}\varepsilon \left(-18B_3R_3R_1^2 - 81B_3R_3^3 - 72B_3R_2^2R_3 - 12R_3\theta_{33}\right.\\
&\quad + B_3\cos(3\phi_1 - \phi_3)R_1^3 - 12B_3R_2^2\cos(\phi_1 - 2\phi_2 + \phi_3)R_1\\
&\quad \left. - 2Q_{32}R_2\sin(\phi_2 - \phi_3)\right),\\
\phi_1' &= \frac{\varepsilon}{8R_1}\left(9B_1R_3\left(R_1^2\sin(3\phi_1 - \phi_3) - 4R_2^2\sin(\phi_1 - 2\phi_2 + \phi_3)\right)\right.\\
&\quad \left. - 2Q_{12}R_2\cos(\phi_1 - \phi_2)\right),\\
\phi_2' &= -\frac{\varepsilon}{8R_2}\left(Q_{21}R_1\cos(\phi_1 - \phi_2) + Q_{23}R_3\cos(\phi_2 - \phi_3)\right.\\
&\quad \left. - 18B_2R_1R_2R_3\sin(\phi_1 - 2\phi_2 + \phi_3)\right),\\
\phi_3' &= -\frac{\varepsilon}{24R_3}\left(B_3\sin(3\phi_1 - \phi_3)R_1^3 + 12B_3R_2^2\sin(\phi_1 - 2\phi_2 + \phi_3)R_1\right.\\
&\quad \left. + 2Q_{32}R_2\cos(\phi_2 - \phi_3)\right). \qquad (18)
\end{aligned}$$

Applying the substitution for the combination angles $\psi_1 = \phi_1 - \phi_2$, $\psi_2 = \phi_2 - \phi_3$, and $\psi_3 = 3\phi_1 - \phi_3$, system (18) becomes:

$$\begin{aligned}
R_1' &= \frac{1}{8}\varepsilon \left(3B_1R_1^3 + 24B_1R_2^2R_1 + 54B_1R_3^2R_1 + 4\theta_{11}R_1 - 9B_1R_1^2R_3\cos(\psi_3)\right.\\
&\quad \left. + 36B_1R_2^2R_3\cos(\psi_1 - \psi_2) - 2Q_{12}R_2\sin(\psi_1)\right),\\
R_2' &= \frac{1}{8}\varepsilon \left(12B_2R_2^3 + 6B_2R_1^2R_2 + 54B_2R_3^2R_2 + 4\theta_{22}R_2\right.\\
&\quad \left. + 18B_2R_1R_3\cos(\psi_1 - \psi_2)R_2 + Q_{21}R_1\sin(\psi_1) - Q_{23}R_3\sin(\psi_2)\right),
\end{aligned}$$

$$
\begin{aligned}
R_3' &= -\frac{1}{24}\varepsilon\left(-18B_3R_3R_1^2 - 81B_3R_3^3 - 72B_3R_2^2R_3 - 12R_3\theta_{33}\right.\\
&\quad \left. + B_3\cos(\psi_3)R_1^3 - 12B_3R_2^2\cos(\psi_1-\psi_2)R_1 - 2Q_{32}R_2\sin(\psi_2)\right),\\
\psi_1' &= \frac{\varepsilon}{8R_1R_2}\left(\left(Q_{21}R_1^2 - 2Q_{12}R_2^2\right)\cos(\psi_1) + R_3\left(Q_{23}R_1\cos(\psi_2)\right.\right.\\
&\quad \left.\left. - 9R_2\left(2\left(B_2R_1^2 + 2B_1R_2^2\right)\sin(\psi_1-\psi_2) - B_1R_1^2\sin(\psi_3)\right)\right)\right),\\
\psi_2' &= \frac{\varepsilon}{24R_2R_3}\left(-3Q_{21}R_1R_3\cos(\psi_1) + \left(2Q_{32}R_2^2 - 3Q_{23}R_3^2\right)\cos(\psi_2)\right.\\
&\quad \left. + R_1R_2\left(B_3\sin(\psi_3)R_1^2 + 6\left(2B_3R_2^2 + 9B_2R_3^2\right)\sin(\psi_1-\psi_2)\right)\right),\\
\psi_3' &= \frac{\varepsilon}{24R_1R_3}\left(\left(B_3R_1^2 + 81B_1R_3^2\right)R_1^2\sin(\psi_3) + 2Q_{32}R_1R_2\cos(\psi_2)\right.\\
&\quad \left. - 18Q_{12}R_2R_3\cos(\psi_1) + 12R_2^2\left(B_3R_1^2 - 27B_1R_3^2\right)\sin(\psi_1-\psi_2)\right). \qquad (19)
\end{aligned}
$$

For more details about how the averaged system and the corresponding asymptotic estimates are obtained, we refer to [23,28] and [29].

4.1 Nontrivial Relative Equilibria

Putting the righthand side of system (19) equal to zero to locate relative equilibria, yields a system of equations which we were unable to solve explicitly. The roots can quite easily be approximated numerically. The isolated roots of the averaged system correspond with 2π-periodic solutions of the original system. In this way, studying periodic solutions becomes the study of the isolated relative equilibria of the averaged system which is much easier and quite straightforward. We choose for this purpose the following representative parameter values $b = \beta_0 = \gamma_0 = U = 1,\ \varepsilon = 0.1$, and find, using a convenient choice of the phase combinations, easily the following relative equilibria:

$$P_1 = (R_1, R_2, R_3, \psi 1, \psi_2, \psi_3) = (0.5131, 0.0554, 0.0045, \pi/2, \pi/2, 0), \qquad (20)$$

$$P_2 = (R_1, R_2, R_3, \psi 1, \psi_2, \psi_3) = (0.4994, 0.0542, 0.0040, \pi/2, \pi/2, \pi). \qquad (21)$$

Linearising system (19) at P_1 and P_2 yields a following matrix of the form:

$$A = \begin{pmatrix} A_1 & \emptyset \\ \emptyset & A_2 \end{pmatrix}, \qquad (22)$$

with $A_i, i = 1, 2$ and $\emptyset 3 \times 3$ matrices.

When studying the dynamics, one considers how the eigenvalues of the matrix A depend on the parameters in order to produce a bifurcation diagram. However, in this case the expressions for the equilibria have not a closed form as a function of the parameters. We shall therefore continue our study numerically.

Note, that we can still significantly reduce the dimension of the parameter space relevant for the bifurcation study. First we easily see that the parameters β_0 and U can be replaced by one parameter, say $\beta = \beta_0 U^2$. This reduces the dimension of the parameter space to 3. We also can get rid of the parameter γ_0 by applying the transformation $\tilde{y}_i = \sqrt{\gamma_0}y_i,\ i = 1, \ldots, 3$ before averaging. This reduces the dimension of the parameter space to 2. Note that this transformation is always possible as γ_0 is assumed to be strictly positive.

One might ask why not study the original system numerically if we are bound to *continue* the study numerically from now on? The advantage of the averaged system is that it indicates with great precision where the periodic solutions are in the form of relative equilibria, regardless of their stability character. Hopf bifurcation of such an equilibrium will then correspond with Neimark–Sacker bifurcation of a periodic solution. For instance, the emergence of 3-tori, as we shall see later on, is detected using continuation software packages like CONTENT [18] or MATCONT [13,14,26]. This is difficult for the original system as the continuation of tori (see [24]) yields many complications owing to dense (Cantorized) sets of resonances.

We use the parameters b and β as control parameters in the bifurcation study. From the eigenvalues of the equilibria at the parameter values mentioned above, we derive that P_1 is a stable node and P_2 is a saddle.

Remark We have not yet proved that we have found all the isolated nontrivial equilibria of the system. Putting this system entirely in software packages like Maple or Mathematica and trying to solve it numerically was not successful. Therefore, we proceed as follows. The last three equations of system (19) can be viewed as linear in the variables $\cos\psi_1,\ \cos\psi_2,\ \sin\psi_3$. Solving this system yields:

$$\cos\psi_1 = \alpha_1 \sin(\psi_1 - \psi_2), \tag{23}$$

$$\cos\psi_2 = \alpha_2 \sin(\psi_1 - \psi_2), \tag{24}$$

$$\sin\psi_3 = \alpha_3 \sin(\psi_1 - \psi_2), \tag{25}$$

with

$$\alpha_1 = \frac{-18\,B_1\,(4\,B_3\,Q_{23} + 9\,B_2\,Q_{32})}{c\,((B_3\,Q_{12}\,Q_{23}) - 9\,B_1\,Q_{21}\,Q_{32})}\,R_2\,R_3, \tag{26}$$

$$\alpha_2 = \frac{18\,B_3\,(B_2\,Q_{12} + 4\,B_1\,Q_{21})}{c\,(B_3\,Q_{12}\,Q_{23} - 9\,B_1\,Q_{21}\,Q_{32})}R_1\,R_2, \tag{27}$$

$$\alpha_3 = \frac{-12\,(B_3\,Q_{12}\,Q_{23} + 3\,(B_2\,Q_{12} + B_1\,Q_{21})\,Q_{32})}{(B_3\,Q_{12}\,Q_{23} - 9\,B_1\,Q_{21}\,Q_{32})}\,\frac{{R_2}^2}{{R_1}^2}. \tag{28}$$

Combining the fact that $\sin(\psi_1 - \psi_2) = \sin\psi_1\cos\psi_2 - \cos\psi_1\sin\psi_2$ with the expressions obtained above for $\cos\psi_1$ and $\sin\psi_1$ we conclude:

Either $\sin(\psi_1 - \psi 2) = 0$, this case yields the equilibria P_1 and P_2, or

$$\sin\psi_1 = \frac{1}{\alpha_2} + \frac{\alpha_1}{\alpha_2}\sin\psi_2. \tag{29}$$

Combining (23) and (24) we get

$$\cos\psi_1 = \frac{\alpha_1}{\alpha_2}\cos\psi_2. \tag{30}$$

Using (29) and (30) and the fact that $\cos\psi_1^2 + \sin\psi_1^2 = 1$, we derive the following formula:

$$\sin\psi_2 = \frac{\alpha_2^2 - \alpha_1^2 - 1}{2\alpha_1}. \tag{31}$$

This expression yields the following formula:

$$\sin\psi_1 = \frac{\alpha_2^2 - \alpha_1^2 + 1}{2\alpha_2}. \tag{32}$$

Combining the expression $\cos(\psi_1-\psi_2) = \cos\psi_1\cos\psi_2+\sin\psi_1\sin\psi_2$ with all the previous results, we give the following expressions:

$$\cos(\psi_1 - \psi_2) = \frac{-1+(\alpha_1^2+\alpha_2^2)}{2\alpha_1\alpha_2}, \tag{33}$$

$$\cos\psi_3 = \pm\sqrt{1-\alpha_3^2\left(1-\cos(\psi_1-\psi_2)^2\right)}. \tag{34}$$

Note, that there are two possibilities for the expression of $\cos(\psi_1 - \psi_2)$:

$$\cos(\psi_1 - \psi_2) = \frac{-1\pm(\alpha_1^2+\alpha_2^2)}{2\alpha_1\alpha_2}.$$

We can however rule out the possibility with the minus sign as it always yields a value outside the interval $[-1, 1]$. Applying the substitution into the first three equations of system (19) yields a polynomial system of three equations with the amplitudes R_1, R_2, R_3 as unknown. This system can be solved numerically. It does not yield any new equilibria.

4.2 Stability of the Relative Equilibrium P_1

Continuing the stable node equilibrium P_1 with respect to the parameter b and β does not yield any interesting bifurcations before hitting the singularity at $R_2 = 0$; see Fig. 4. To avoid this singularity, which is inherent to phase-amplitude coordinates, we use the following nonsingular coordinate transformation before averaging and continue the corresponding isolated nontrivial equilibrium P_1.

$$x_i = x_{i1}\cos(i\omega_0 t) + \frac{x_{i2}}{i\omega_0}\sin(i\omega_0 t), \quad i = 1,\ldots,3. \tag{35}$$

The continuation of P_1 in these new coordinates yields two 'different' Hopf bifurcations. See Fig. 4. Because of symmetry, twice as many Hopf bifurcations are detected. These correspond however with the same object, a 2-torus, and consequently need not be studied separately.

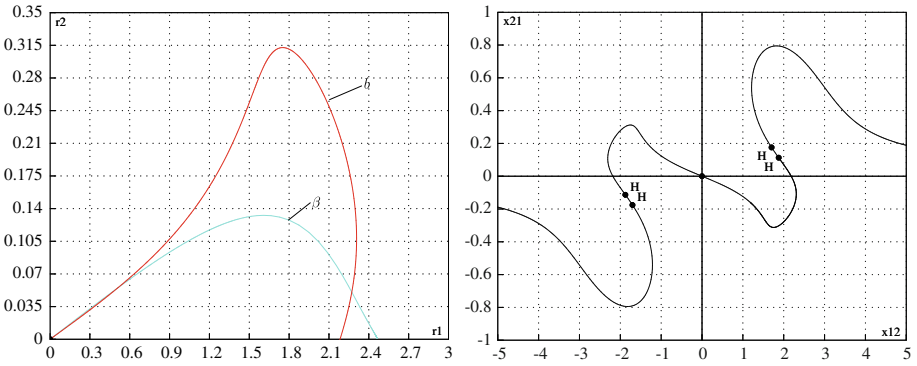

Fig. 4 Continuation of the equilibrium P_1 with respect to the parameters b and β in nonsingular coordinates (35) projected onto the R_1R_2-plane (*left*). The letters mean that the curve was obtained by continuation with respect to that parameter. No bifurcations were detected except a branching point at the origin. This picture is however incomplete as we cross the singularity $R_2 = 0$. Continuation of P_1 in the more suitable variables (*right*). The bifurcations which are symmetrically situated with respect to the origin should be identified because of the $\mathbb{Z}_2$ symmetry in the averaged vector field. They correspond with the same object. The first quadrant in the $R_1 - R_2$ coordinates corresponds with the second quadrant in the $x_{12} - x_{21}$ coordinates

The first Hopf bifurcation is subcritical and occurs at the critical value $b_1 = -0.052101$ with first Lyapunov coefficient $l_1 = 4.898 \cdot 10^{-2}$. Below this critical value of b the, at that moment, unstable equilibrium P_1 undergoes once again a Hopf bifurcation (this time a supercritical one), at the critical value $b_2 = -0.05453$ with corresponding Lyapunov coefficient $l_1 = -2.861$. In both cases the cycle emerging from this Hopf is unstable. (Note that we use the term 'cycle' in the sense of closed curve or circle.) Continuation of P_1 with respect to the parameter b in the opposite direction yields nothing special. The equilibrium P_1 collides with the origin at the value $b = 1.065$.

Remark At the second Hopf bifurcation the first Lyapunov coefficient is negative which means the emerging cycle is stable on the centre manifold. In this case however the centre manifold itself is unstable as the equilibrium P_1 is unstable in the full phase-space. Consequently the emerging cycle is unstable.

It is known from the theory of averaging that nondegenerate Hopf bifurcations of the isolated nontrivial equilibria in the averaged system correspond with Neimark–Sacker bifurcations of the corresponding periodic solution in the original system yielding stable or unstable 2-tori, depending on the normal form coefficient at the bifurcation point and the stability of the centre manifold.

4.3 Stability of the Relative Equilibrium P_2

Continuation of this equilibrium yields two subcritical Hopf bifurcations. The first one occurs at the parameter value $b_{c_1} = 0.0824$ with first Lyapunov coefficient $l_1 = 0.631$ and emerging frequency equal to $\omega_{h_1} = 0.00747$. The second Hopf-bifurcation occurs at $b_{c_2} = 0.0108$ with corresponding first Lyapunov coefficient $l_1 = 0.550$ and emerging frequency equal to $\omega_{h_2} = 0.0108$.

The unstable cycle emerging from the first bifurcation is continued with respect to the parameter b, see Fig. 5. This cycle undergoes first a fold bifurcation at the parameter value $b = 0.0899$ then, after a branching point bifurcation at $b = 0.0784$, the cycle stabilizes and becomes hyperbolic yielding a stable 2-torus in the corresponding original system. This torus was numerically localized in the original system as well, see Fig. 6. Because of the normal hyperbolicity of the cycle in the averaged system, we have persistence and therefore the torus can be traced in the original system despite the higher order terms omitted by averaging.

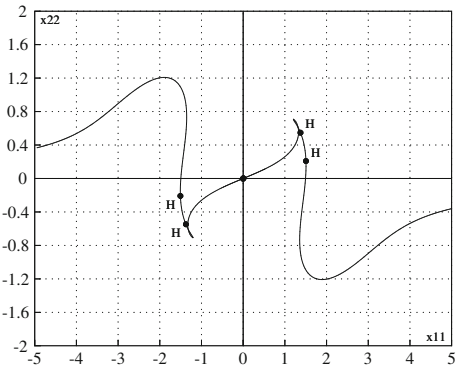

Fig. 5 Continuation of the equilibrium P_2 with respect to the parameter b projected onto the $x_{11}x_{22}$-plane. Two Hopf bifurcations were detected, the first one is subcritical and the second one supercritical. The bifurcations which are symmetrically situated with respect to the origin should be, because of the $\mathbb{Z}_2$ symmetry in the averaged vector field, identified. They correspond with the same object

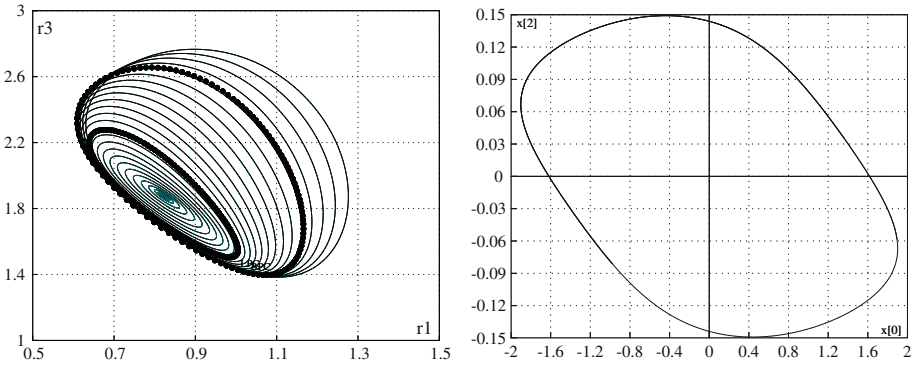

Fig. 6 Continuation of the cycle emerging from the first Hopf-bifurcation of P_2. The small *black* cycle corresponds with the fold bifurcation, the bigger one corresponds with the branching bifurcation after which the cycle stabilises, yielding a 2-torus in the corresponding original system (17) (*left*). Stroboscopic Poincaré section of the original system projected onto the x_1x_2-plane shows the presence of a stable 2-torus with $\varepsilon = 0.05,\ b = 0.0755,\ \beta = 1.1$ (*right*)

5 Bifurcation Diagrams in the Parametric Excitation Case $\omega = \sqrt{k_1}\omega_0$

It has been shown in [11,9,20] and [31] that when quasi-periodic solutions are involved, the set of possible bifurcations in parameter space can be very complex. In general there will be an infinite number of Arnold resonance tongues, the bifurcation sets are expected to be of fractal nature. This complexity will take of course different forms for explicit mechanical (dynamical) systems, depending on symmetry and other modeling assumptions.

In what follows, we shall first study in detail the codimension one and codimension two bifurcations of the normal form (the first averaged system to first order); then we return to the original system to see how many of these bifurcations survive the addition of higher order terms. In order to avoid singularities that occur using the phase-amplitude coordinates, we shall from now on use the more suitable nonsingular coordinates as given by Eq. (35). The averaged system in these new coordinates is given in appendix 1. The averaged system has two 3D invariant manifolds.

$$\Sigma_1 = \left\{\{x_{11}, x_{12}, x_{21}, x_{22}, x_{31}, x_{32}\} \in \mathbb{R}^6,\ x_{11} = x_{22} = x_{31} = 0\right\} \text{ and,}$$

$$\Sigma_2 = \left\{\{x_{11}, x_{12}, x_{21}, x_{22}, x_{31}, x_{32}\} \in \mathbb{R}^6,\ x_{12} = x_{21} = x_{32} = 0\right\}.$$

The stable relative equilibrium P_1 found in the preceding section lies on the invariant manifold Σ_1, the unstable relative equilibrium P_2 on Σ_2.

The main bifurcation diagram was obtained using MATCONT 2.2.9 under Matlab 7. How this bifurcation diagram is built up is explained in the captions of Fig. 7 and 8. The terminology on bifurcations is not uniform in the literature. Because of the use of MATCONT, we shall adopt here more or less the same notation as in [17] to establish which scenario holds in our case. To assist the reader we will regularly indicate other nomenclatures between brackets.

Consider Fig. 7. Various codimension one and two bifurcations were detected. A prominent one involves the relative equilibrium P_2 and occurs at the parameter values $b = 0.056$ and $\beta = 1.447$. The normal form, of the averaged system, around this codimension 2 bifurcation, usually referred to as the Hopf-Hopf (HH) bifurcation, has been studied in detail;

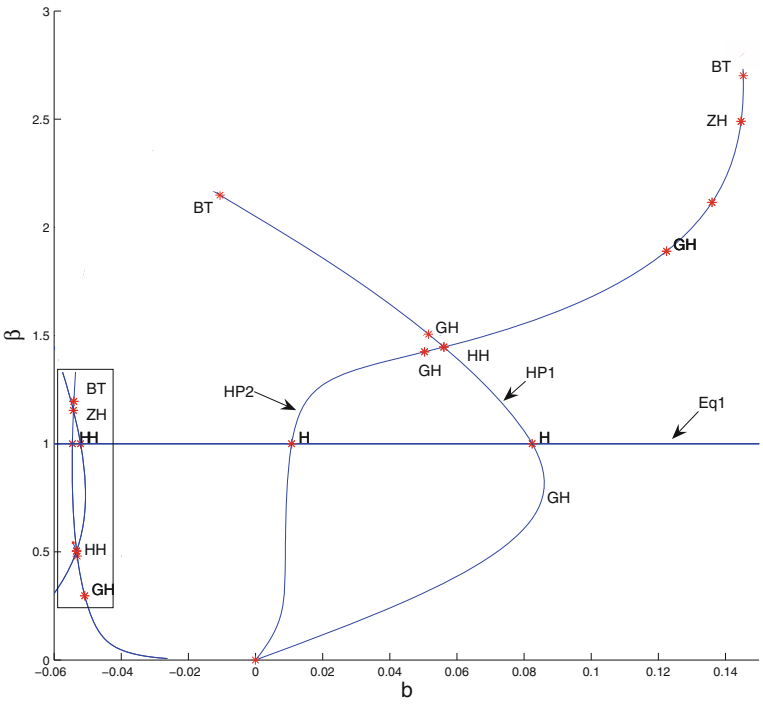

Fig. 7 Bifurcation diagram of the averaged system. Starting on the *horizontal line* (*Eq1*), the unstable relative equilibrium P_2 is continued with respect to the parameter b. Two Hopf bifurcations were detected, indicated by *H*. Continuation of the two Hopf points yields the curves *HP1* and *HP2*. Various codimension two bifurcations are detected on the curves HP1 and HP2 among which a generalised Hopf bifurcation (*GH*), a fold–Hopf bifurcation (also known as zero-Hopf or *ZH*), a Bogdanov–Takens bifurcation (*BT*) as well as a Hopf–Hopf bifurcation (*HH*). More to the left, we find the bifurcation curves involving the stable relative equilibrium P_1. See Fig. 8 for more details and a magnification of the *rectangular area*

see for example [17]. In this case, the relative equilibrium has two pairs of purely imaginary eigenvalues $\lambda_{1,4} = \pm i\omega_1$, and $\lambda_{2,3} = \pm i\omega_2$, with $\omega_1 \neq \omega_2$ and satisfying certain nondegeneracy conditions. We refer to [17] for all the topologically different cases that may occur in the vicinity of this bifurcation. Various bifurcation branches lead on from the bifurcation point HH; for details see the caption of Fig. 7.

In the notation of [17]: Analysing the normal form coefficients of the nontrivial relative equilibrium P_2, computed with MATCONT, we find:

$$p_{11}p_{22} = -1,\ \theta = -2.430,\ \delta = -24.494,\ \Theta = -1.017 \times 10^3 \text{ and } \Delta = 1.160 \times 10^5.$$

From these coefficients one can establish that we have the case $p_{11}p_{22} < 0$ under subcase 4. This means the presence of a $\mathbb{T}^2$ torus in the vicinity of the Hopf–Hopf bifurcation corresponding with a $\mathbb{T}^3$ torus in the original system. This torus is unstable because the equilibrium P_2 was unstable, yielding an unstable centre manifold on which the torus lies. Consequently this torus is numerically 'undetectable'

The second Hopf–Hopf bifurcation involves the stable equilibrium P_1 and occurs at the parameter values $b = -0.05328$ and $\beta = 0.5038$ with the following normal form coefficients:

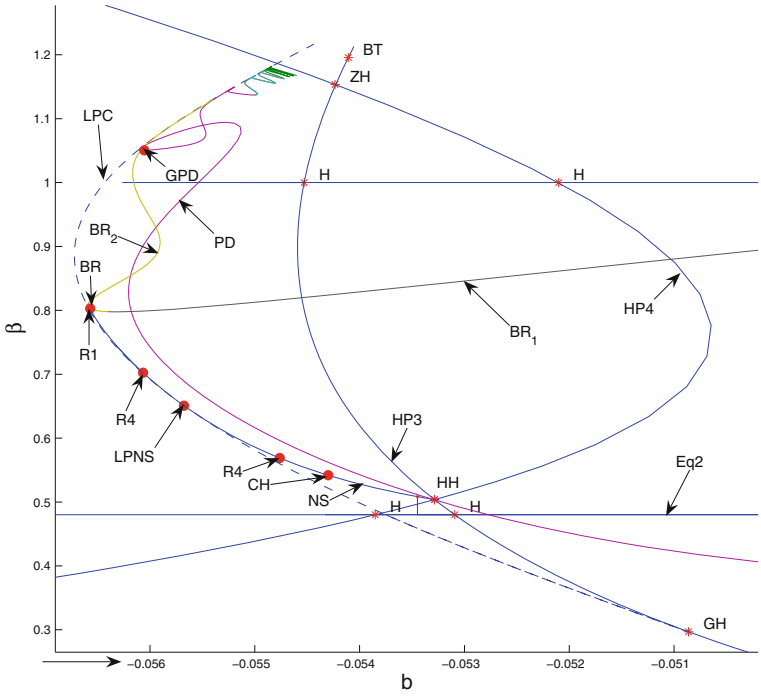

Fig. 8 Magnification of the *rectangular area* in Fig. 7 shows the bifurcations involving the stable relative equilibrium P_1. There are two Hopf bifurcation curves (*HP3*) and (*HP4*), also various codimension two bifurcation points were detected. Starting on the *horizontal line* (*Eq2*), the stable relative equilibrium is continued. After hitting the Hopf curve HP3, the stable emerging cycle is continued in the *horizontal direction* with respect to the parameter b until we hit the fold bifurcation where this cycle collides with an unstable one and vanishes. The locus of the fold (*saddle-node*) points is indicated by curve LPC. Before hitting the *fold curve* at $b = -0.053447955$, the cycle was continued in the *vertical direction* with respect to the parameter β. A Neimark–Sacker bifurcation is detected. The Neimark–Sacker curve (*NS*) is obtained from this point by continuation. The point CH indicates a Chenciner (also called degenerate NS bifurcation). The point R4 indicates a 1:4 resonance and the point LPNS corresponds with a fold–Neimark–Sacker bifurcation where the curves LPC and NS cross. After the Neimark–Sacker bifurcation, the cycle undergoes a period-doubling bifurcation, the locus of which is indicated by the *curve* (*PD*). The PD curve shows remarkable behaviour in the sense that there is an accumulation of unusual period-doubling points to a segment in the parameter space

$$p_{11}p_{22} = -1,\ \theta = 6.013,\ \delta = 0.970,\ \Theta = 2.720 \times 10^4 \text{ and } \Delta = 64.380 \times 10^5.$$

We will zoom in into the neighborhood of the Hopf–Hopf bifurcation of P_1 in Fig. 8. This case as well yields a 2-torus in the neighborhood of the Hopf–Hopf bifurcation as it corresponds , according to [17], to the case $p_{11}p_{22} < 0$ under subcase 2. The 2-torus which should be called a 'relative torus', corresponds with a 3-torus in the original system; it is stable as it has a negative Lyapunov coefficient. This means the torus is numerically detectable.

We find the following interesting codimension one and two bifurcations:

NS-bifurcation Continuing with respect to the parameter b and the stable nontrivial equilibrium starting at the values $b = -.04,\ \beta = 0.48$, we hit the Hopf line at the parameter value $b = -0.053091803$. The bifurcation is supercritical. The stable cycle L_s emerging from this bifurcation is then continued until the value $b = -0.053447955$. This cycle is then continued

with respect to the parameter β. A supercritical Neimark–Sacker bifurcation is detected at the parameter value $\beta = 0.50846183$ yielding a 2-torus in the averaged system corresponding with a 3-torus in the original system. The locus of these Neimark-Sacker points is indicated by the curve (NS). See Fig. 8 and 13 (also discussed in the next section).

Fold bifurcation (saddle–node) From the generalised Hopf point emanates an LPC curve where the stable cycle L_s collides with the unstable one,L_u, and vanishes. See the dashed curve in Fig. 8.

Chenciner bifurcation (degenerate NS) On the Neimark–Sacker curve, there is a Chenciner bifurcation point at the parameter values $b = -0.0543$ and $\beta = 0.5420$. Here the Neimark–Sacker bifurcation changes from supercritical (for $b > -0.0543$) to subcritical.

The 1:4 resonance On the Neimark–Sacker curve we hit twice the strong 1:4 resonance (R4) at the parameter values $b = -0.0548$, $\beta = 0.5688$ and again at the values $b = -0.0561$ and $\beta = 0.7024$.

The 1:1 resonance The Neimark-Sacker curve ends at the point labeled R1. Here, the complex conjugate multipliers on the unit circle collide and become both equal to 1.

The Fold-Neimark–Sacker bifurcation The LPC curve and the NS curve cross at the parameter values $b = -0.055675192$ and $\beta = 0.65078135$ yielding a Fold–Neimark–Sacker (LPNS) bifurcation where two multipliers are complex and on the unit circle and a third multiplier is real and equals 1. This occurs at the parameter values $b = -0.056576$ and $\beta = 0.80280$.

Branching point bifurcation A cycle branches from L_u along the curve BR_1. Another cycle branches from L_s along the curve BR_2. These two curves emanate from the point labeled BR on the LPC curve which lies too close to be distinguished from the 1:1 resonance point R1 on the Neimark–Sacker curve; see Fig. 8.

Accumulation of pitchfork-flip, generalised PD and 1:2 resonance When continuing the cycle L_s, emerging from the Hopf bifurcation at $b = -0.05453$ and $\beta = 1$, with respect to the parameter b until the value $b = -0.055$, then with respect to the parameter β, it undergoes a supercritical period doubling bifurcation at the value $b = -0.055$, $\beta = 1.1371$. An unstable period 2 cycle emerges corresponding with a 2-torus (double torus) in the original system. The period-doubling curve is continued using AUTO[15]; see Fig. 8. Remarkably enough we observe a repetitive pattern of codimension two bifurcations. A sequence of respectively generalised period doubling (GPD), pitchfork-flip (LPPD), 1:2 resonance (R2), generalised period doubling (GPD), 1:2 resonance (R2) and pitchfork-flip (LPPD) keeps repeating and accumulating in the parameter space. See for this phenomenon Fig. 9. This is an interesting and new bifurcation sequence, the dynamics of which we do not quite understand. The accumulation is due to the presence of a saddle-node homoclinic bifurcation, see Fig. 10 and next item. It might be very interesting to generate a map exhibiting these properties and study it in detail to improve our understanding. Note that this phenomenon involving the period doubling curve occurs entirely on the invariant 3D manifold Σ_1. The period 2 cycle emerging from the period doubling of the cycle L_s does however not belong to Σ_1. This means that the restriction of the flow to Σ_1 does not yield this remarkable period doubling curve. Another interesting question might be whether this particular sequence of codimension two bifurcations is universal, at least in systems with this symmetry.

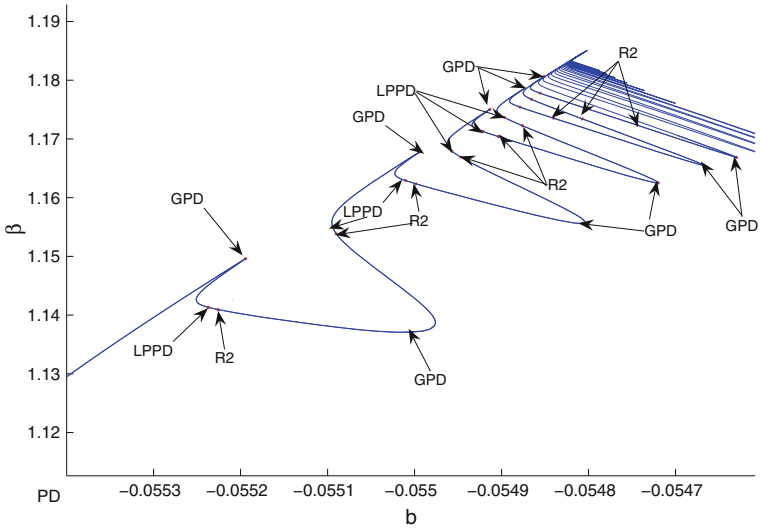

Fig. 9 Magnification of the period doubling curve in the vicinity of the accumulation region showing a repetitive pattern of the following codimension two bifurcations occurring alternatively: *GPD* (generalised period doubling), *LPPD* (pitchfork-flip) bifurcation, *R2* (1:2 resonance), GPD, R2 and LPPD. As we approach the accumulation region in the parameter space, the period of the cycle L_s grows rapidly resulting in the emergence of a saddle-node homoclinic orbit connecting a nonhyperbolic nontrivial equilibrium to itself. See Fig. 10

Saddle-node homoclinic bifurcation In region I, see Fig. 10, two extra nontrivial equilibria emerge and disappear along the fold curves f_1 and f_2 that coalesce at the cusp point. On the line segment C_1C_2 the nonhyperbolic, nontrivial equilibrium has a saddle-node homoclinic orbit. Continuation of this saddle-node homoclinic orbit yields the curve (HOM). At the codimension two bifurcation points C_1 and C_2, the homoclinic orbit to the saddle-node becomes non-central, meaning, in this case, that it returns to the equilibrium along the stable manifold forming a nonsmooth loop. Using our toolboxes, we can switch between saddle-node and saddle homoclinic orbits. This results in a sharp, but smooth turn to the right of the curve (HOM) after passing the point C_1 where it approaches the LPC curve. After performing the switch at the codimension two point C_2, the homoclinic curve is continued. We observe that it approaches the Bogdanov-Takens point, see Fig. 10. The corresponding homoclinic loops in the three situations (i.e. between the BT point and C_1, between C_1 and C_2 and after passing the point C_2) are given in phase-space in Fig. 11.

NS-bifurcation of the double period orbit Continuing the cycle L_s emerging from the Hopf bifurcation at $b = -0.05453$ and $\beta = 1$, with respect to the parameter b until the value $b = -0.055$, then with respect to the parameter β, the cycle undergoes a period doubling bifurcation at the value $b = -0.055,\ \beta = 1.1371$. The unstable period 2 cycle is continued with respect to the parameter β. A supercritical Neimark–Sacker bifurcation is detected at the parameter values $b = -0.0550039,\ \beta = 1.137694$, yielding a stable 2-torus in the averaged system corresponding with a 3-torus in the original system, see Fig. 12. This torus, as we shall see later, eventually breaks up according to Shilnikov's scenario [2], yielding a strange attractor.

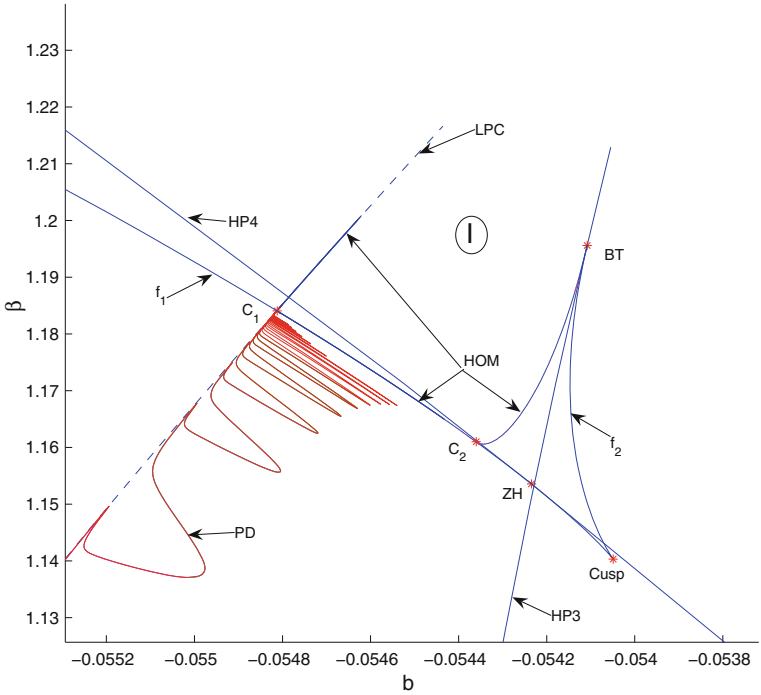

Fig. 10 Parametric portrait of the normal form in the vicinity of the accumulation region. In region I, the cycle L_s has disappeared by the homoclinic bifurcation. Instead two nontrivial equilibria emerge and vanish along the fold curves f_1 and f_2. On the curve (HOM) there are two codimension two bifurcation points C_1 and C_2 where the homoclinic orbit becomes non-central as it looses smoothness because it returns to the equilibrium along the stable manifold

6 Torus Bifurcations in the Parametric Excitation Case $\omega = \sqrt{k_1}\omega_0$

We consider some of the bifurcations of the preceding section in more detail.

6.1 The Torus Emerging from the Hopf–Hopf Bifurcation

Figure 13 shows the Poincaré section of the orbits through the section $\Sigma = \{\{x_{11}, x_{12}, x_{21}, x_{22}, x_{31}, x_{32}\} \in \mathbb{R}^6, x_{11} = 0\}$ in the vicinity of the NS curve involving the period 1 cycle in the neighborhood of the Hopf–Hopf bifurcation. The closed curve in the Poincaré section confirms the presence of the stable 2-torus in the averaged system as predicted by the normal form analysis, see Fig. 13; it is a 'relative torus' and corresponds with a 3-torus in the original system. The computation of the Lyapunov exponents confirms the torus character of the closed curve. We found the following Lyapunov exponents: $\lambda_1 = -1.4 \times 10^{-5}$, $\lambda_2 = -1.8 \times 10^{-5}$, $\lambda_3 \approx \lambda_4 = -4.0 \times 10^{-3}$, $\lambda_5 = -2.0$, and $\lambda_6 = -2.4$. The Poincaré section Σ will in what follows always be used as cross-section.

6.2 Torus Doubling from Period 1 Cycle

The 2-torus in the averaged system emerging from the Neimark–Sacker bifurcation of the period 1 cycle undergoes one torus doubling, see Fig. 14. The Lyapunov exponents are as

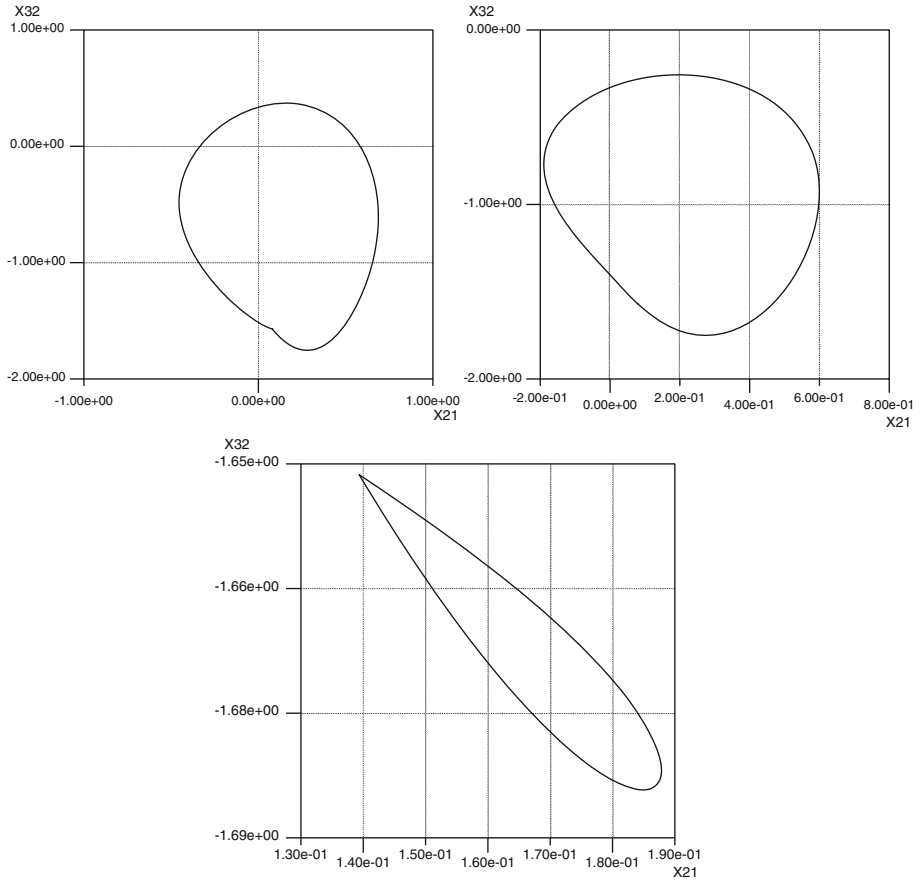

Fig. 11 Phase portrait of the nonsmooth homoclinic orbit (*upper left*) projected onto the $x_{21}x_{32}$ plane with $b = -0.0547168,\ \beta = 1.1925$. corresponding in the parameter space to a point on the HOM curve, somewhere between C_1 and the LPC curve. The *upper right figure* shows a saddle-node homoclinic orbit somewhere along the *line segment* C_1C_2, $b = -0.054778,\ \beta = 1.1824$. The last figure shows a nonsmooth homoclinic orbit with $b = -0.054202,\ \beta = 1.1735$. corresponding, in the parameter space, to a point on the segment of the curve HOM connecting the point C_2 with the Bogdanov-Takens point

follows: $\lambda_1 \approx \lambda_2 = O(10^{-5}),\ \lambda_3 = -5.7 \times 10^{-4},\ \lambda_4 = -5.7 \times 10^{-3}, \lambda_5 = -2.0$ and $\lambda_6 = -2.4$. After that, the torus eventually breaks up by loosing smoothness, through a loss of normal hyperbolicity, leading to the birth of a strange attractor. The Figs. 15, 16, 17 show how this happens. After the period doubling has occurred, and as the parameter β varies, we enter once the 1:17 Arnold tongue near $\beta = 0.5735$, and leave it without detecting any interesting bifurcation. The torus was immediately detectable and smooth when passing the tongue. We have therefore omitted this from the sequence of figures.

6.3 Torus Doubling from Period 2 Cycle

For this purpose we keep the parameter $b = -0.0550039$ constant and vary the parameter β. After a sequence of phase lockings where we cross numerous Arnold tongues, we end up at the 1:11 resonance tongue of the fifth iterate of the Poincaré map around the parameter value

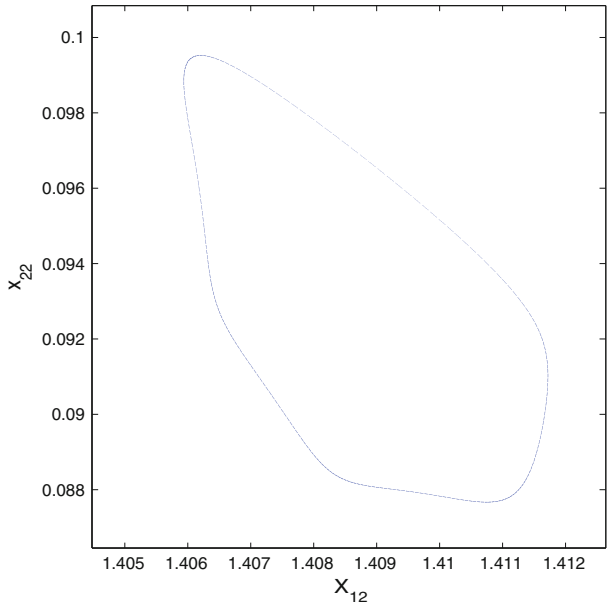

Fig. 12 Poincaré section of the averaged system projected onto the (x_{12}, x_{22}) plane, with $x_{11} = 0$ as a cross-section at the parameter values $b = -0.0550039$, $\beta = 1.13768$. The Neimark–Sacker bifurcations took place at the parameter values $b = -0.0550039$ and $\beta = 1.1377694$. Above this value of β there is a stable period 2 cycle corresponding with a stable 2-torus in the original system. Below this value of β, there is a stable 2-torus ('relative torus') in the averaged system. The *closed curve* shows the torus in the averaged system corresponding with a 3-torus in the original system

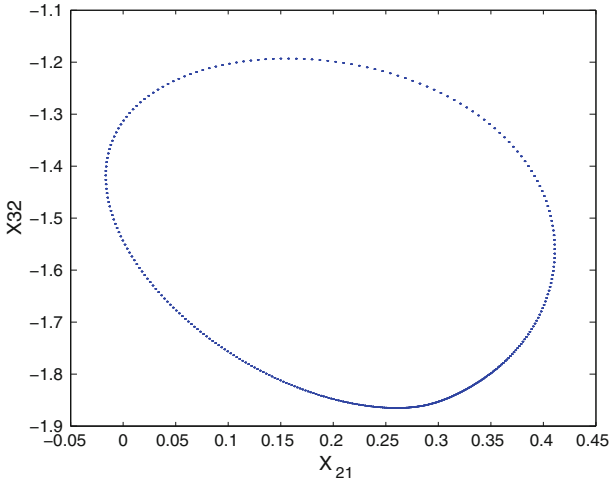

Fig. 13 Projection of the Poincaré section onto the (x_{21}, x_{32}) plane showing a smooth stable 2-torus in the averaged system in the vicinity of the Hopf–Hopf bifurcation, $b = -0.0534$, $\beta = 0.56$, corresponding to a 3-torus in the original system

$\beta = 1.1376769$. If one wishes to generate a figure, the Runge-Kutta (78) integration scheme can be used. To view the closed curve one should follow the unstable manifolds of the saddles. See for example the results of Krauskopf and Osinga [16]. We omit the figure. At the parameter

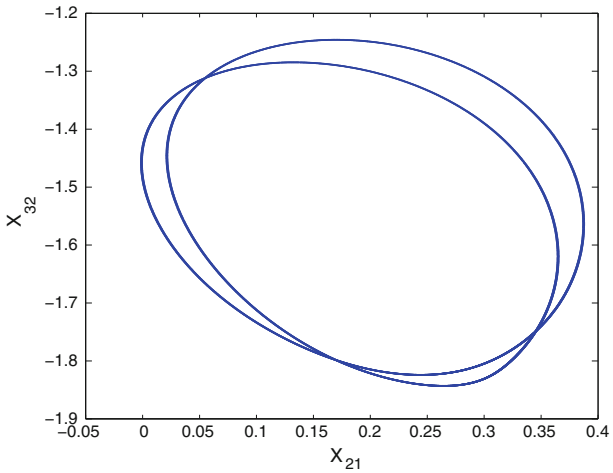

Fig. 14 Poincaré section projected onto the (x_{21}, x_{32}) plane showing a smooth double $\mathbb{T}^2$ torus just after the period-doubling has occurred, $b = -0.0534$, $\beta = 0.57$. The Lyapunov exponents are: $\lambda_1 \approx \lambda_2 = O(10^{-5})$, $\lambda_3 = -5.7 \times 10^{-4}$, $\lambda_4 = -5.7 \times 10^{-3}$, $\lambda_5 = -2.0$ and $\lambda_6 = -2.4$

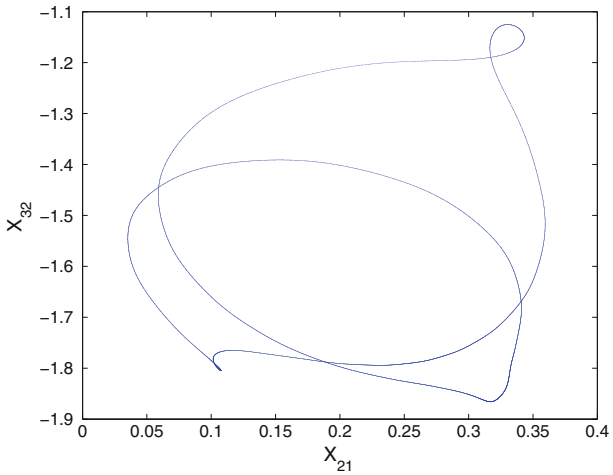

Fig. 15 Poincaré section projected onto the (x_{21}, x_{32}) plane showing the double $\mathbb{T}^2$ torus becoming more deformed and starting gradually to loose normal hyperbolicity as λ_3 becomes close to zero. $b = -0.0534$, $\beta = 0.5742$. $\lambda_1 \approx \lambda_2 \approx 0$, $\lambda_3 = -8.0 \times 10^{-4}$, $\lambda_4 = -8.3 \times 10^{-4}$, $\lambda_5 = -2.0$ and $\lambda_6 = -2.4$.

value $\beta = 1.13767675$ the phase locked periodic solution undergoes a period doubling bifurcation in the direction of the unstable manifolds of the saddles. At this stage the period 2 torus is completely destroyed according to one of the scenarios described in [2]. Decreasing the parameter even further we observe the emergence of a strange attractor, see Fig. 18.

7 The Original System in the Parametric Excitation Case $\omega = \sqrt{k_1}\omega_0$

In order to study for reasons of comparison the original system, we consider the time-periodic Poincaré map using the same parameter values as in the averaged system i.e. $b = 1$, $\beta = 1$

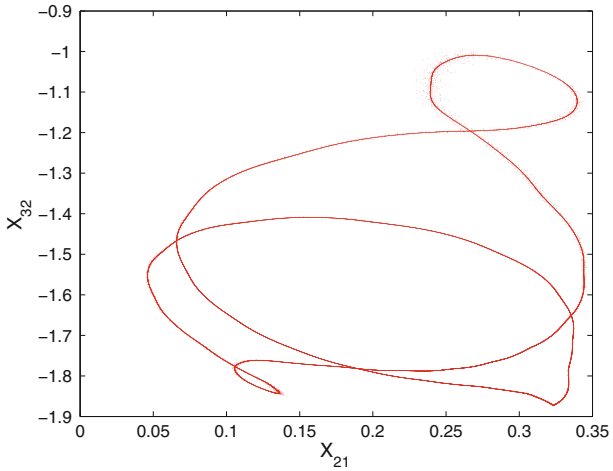

Fig. 16 Poincaré section projected onto the (x_{21}, x_{32}) plane showing loss of normal hyperbolicity of the double $\mathbb{T}^2$ torus, $b = -0.0534,\ \beta = 0.575$. $\lambda_1 \approx \lambda_2 \approx \lambda_3 \approx 0, \lambda_4 = -1.7 \times 10^{-4}, \lambda_5 = -2.0, \lambda_6 = -2.4$.

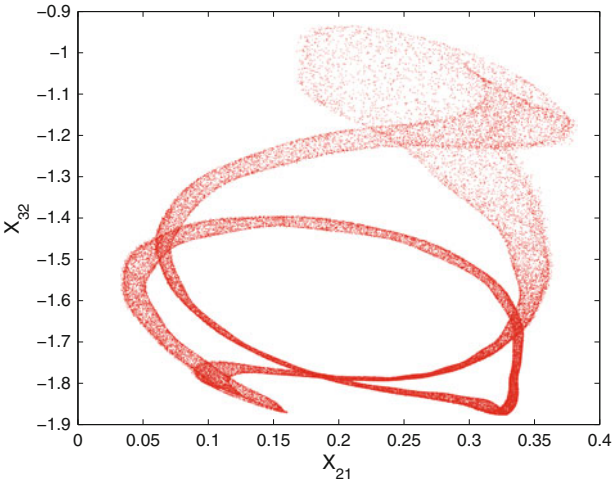

Fig. 17 Poincaré section using Σ as cross-section showing the strange attractor emerging after the torus has been destroyed. $b = -0.0534,\ \beta = 0.576$. The fact that two of the six Lyapunov exponents are still equal to zero indicates that the remnants of the torus are still involved in the dynamics within the attractor. We found $\lambda_1 = 1.8 \times 10^{-4}, \lambda_2 \approx \lambda_3 \approx 0, \lambda_4 = -4.4 \times 10^{-4}, \lambda_5 = -2.0, \lambda_6 = -2.4$. The Kaplan-Yorke dimension, $D_{KY} = 3.4$.

and $\varepsilon = 0.1$. Note that the original system and consequently the original system in quasi-normal form (17) possesses a $\mathbb{Z}_2$ symmetry, i.e. it is invariant with respect to the following transformation:

$$T : \begin{pmatrix} x_1 \\ x_2 \\ x_3 \end{pmatrix} \mapsto \begin{pmatrix} -x_1 \\ -x_2 \\ -x_3 \end{pmatrix}.$$

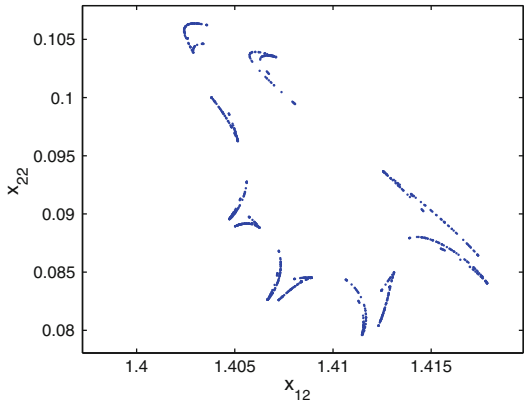

Fig. 18 Numerically computed Poincaré section of the period 2 torus using $x_{11} = 0$ as cross-section in the 1:11 resonance tongue at the parameter values $b = -0.0550039$, $\beta = 1.1376769$ showing the presence of a strange attractor

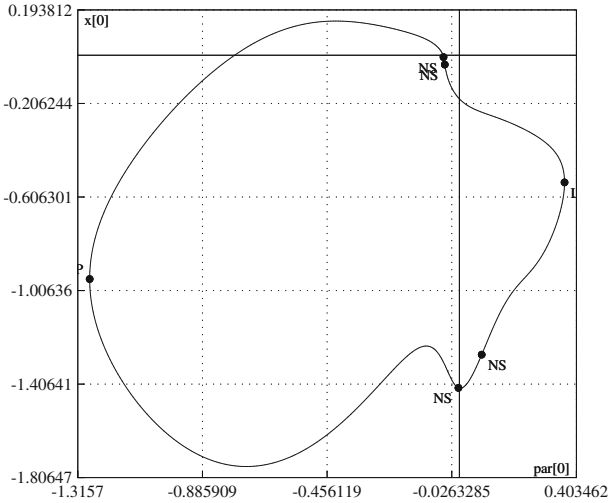

Fig. 19 Time-periodic Poincaré section plotted onto the $b - x_1$ plane obtained by CONTENT using the original system (17) through continuation with respect to the parameter b of the stable equilibrium, corresponding with the 2π-periodic solution. $\varepsilon = 0.1$, NS stands for Neimark–Sacker bifurcation and LP stands for fold bifurcation. The fold points are absent in the averaged system

7.1 The Neimark–Sacker Bifurcation of the 2π-Periodic Solution

A stable fixed point, corresponding with a 2π-periodic solution, was detected using the software package CONTENT [18]. Continuation with respect to the parameter b yields two Neimark–Sacker bifurcations: at the value $b = -0.0504$, averaging-normalization gives a Hopf bifurcation of the stable equilibrium at $b = -0.052101$; at the second value, $b = -0.0548$, averaging-normalization produces $b = -0.0545$.

The unstable cycle is found through further continuation with respect to the parameter b. After hitting the fold bifurcation, the unstable cycle is located. This cycle undergoes two Neimark–Sacker bifurcations: at $b = -0.0033$, the unstable relative equilibrium by averaging produces $b = -0.0824$; the second one at $b = 0.077$, by averaging we find $b = 0.0108$.. See Fig. 19.

Note that the normal form method of averaging predicted the bifurcation points of the stable solutions with good accuracy. This accuracy improves, as predicted by the theorems on averaging, when decreasing the value of the parameter ε or by computing higher-order normal forms. We took $\varepsilon = 0.1$ which is too large for an $O(\varepsilon)$ approximation of these bifurcation values. Taking $\varepsilon = 0.05$ for example yields the following parameter values where the Neimark-Sacker bifurcation predicted by averaging-normalization took place. We found that the stable cycle undergoes a Neimark-Sacker bifurcation at $b = -0.00548$ and at $b = -0.0504$. The unstable cycle undergoes a Neimark-Sacker bifurcation at $b = 0.0056$ and at $b = 0.08$. We see that the accuracy regarding the predicted bifurcation values of the unstable cycle has significantly improved by just halving ε.

Bifurcation Diagrams and the Emergence of 3-Tori

We computed a bifurcation diagram by CONTENT [18] using system (17). When considering the stroboscopic Poincaré map, the periodic orbit corresponding with the nontrivial equilibrium P_1 of system (18) is first numerically spotted and then continued with respect to the parameter b. Exactly the same procedure was carried out as in the case of the averaged system. All the dynamics present in the original system is very well captured by the averaged system. The bifurcation diagram in Fig. 7 is similar to that of the original system. As an indication of how well the averaged system approximates the original one, we give here the parameter values where the double-Neimark–Sacker bifurcation (NS–NS) occurs and the corresponding parameter values of the Hopf–Hopf (HH) bifurcation in the averaged system for $\varepsilon = 0.1$.

The double Neimark-Sacker (NS–NS) in the original system occurs at $b = -0.05322$, $\beta = 0.5017$ and the Hopf–Hopf in the averaged system occurs at $b = -0.05328$, $\beta = 0.5038$. This is a rather good approximation. The stable 3-torus as well as the double 3-torus emerging from respectively the double-Neimark–Sacker bifurcation and the supercritical torus doubling as predicted by the normal form were numerically localized in the original system. See Fig. 20.

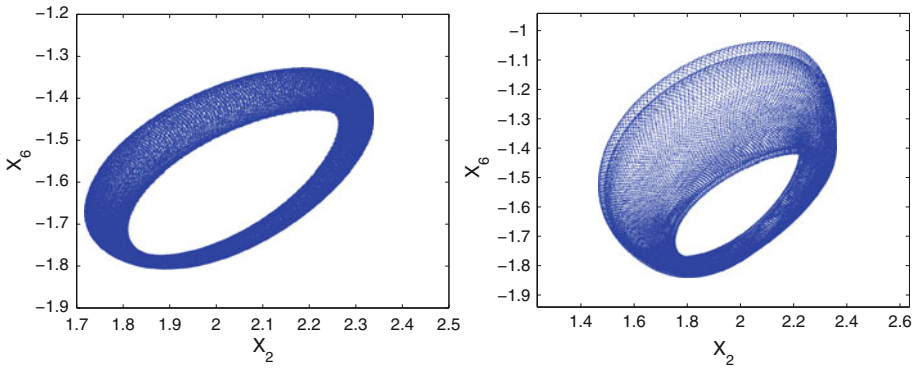

Fig. 20 Time-periodic Poincaré section projected onto the plane x_2x_6 showing the presence of a stable 3-torus (*left*) in the original system in the vicinity of the NS–NS bifurcation, as predicted by the normal form. To generate this figure, the Runge-Kutta (78) integration scheme was used with the following initial conditions $\varepsilon = 0.1$, $b = -0.0534$, $\beta = 0.52$, $x_1 = 0.1635$, $x_2 = 2.3570$, $x_3 = 0.0638$, $x_4 = -0.0680$, $x_5 = -0.1264$, and $x_6 = -1.3430$. The flow was integrated over the time interval $t \in [0, 0, 5 \times 10^5]$. A stable double 3-torus (*right*) emerged after a period doubling of the 3-torus (*left*). To generate this figure, the Runge-Kutta (78) integration scheme was used with the following initial conditions $\varepsilon = 0.1$, $b = -0.0534$, $\beta = 0.57$, $x_1 = 0.1635$, $x_2 = 2.3570$, $x_3 = 0.0638$, $x_4 = -0.0680$, $x_5 = -0.1264$, and $x_6 = -1.3430$. The flow was integrated over the same time interval $t \in [0, 0.5 \times 10^5]$

Table 1 Frequency analysis of the data obtained by integrating the original system showing the presence of a double $\mathbb{T}^3$ torus

ω	Frequency	Amplitude
ω_1	7.804718971343821e-03	3.104569561705033e-01
ω_2	9.369393216950331e-03	1.443367758753760e-01
$\omega_2 - \omega_1$	1.564660658988895e-03	2.978702176331686e-02
$\omega_2 + \omega_1$	1.717409259141677e-02	1.590363241756515e-02
$2\omega_2 - \omega_1$	1.093407933327835e-02	1.479297670093936e-02
$2\omega_1 - \omega_2$	6.240029591658622e-03	1.358047157776031e-02
$2\omega_2$	1.873875305580177e-02	9.621203439704008e-03
$2\omega_1$	1.560941256009615e-02	7.737656805482373e-03
$2\omega_2 + \omega_1$	2.654347195181721e-02	2.534263314754040e-03
$2\omega_1 + \omega_2$	2.497882520003850e-02	2.033942947810174e-03

A frequency analysis was performed on the data to establish the presence of the 3-torus. Two extra frequencies were found in the data. This indicates that the object in Fig. 20 can be identified as a 3-torus. See Table 1.

7.2 Qualitative Differences

Choosing the parameter ε relatively large, $\varepsilon = 0.1$, the original system shows topological differences from its normal form; see Figs. 19 and 21. The fold bifurcations detected are not present in the normal form. Outside this range of the parameter b the periodic solutions disappear but in the normal form they are still present. This is due to the fact that the parameter ε is too big to guarantee applicability of the corresponding theorems. Altogether, inside the

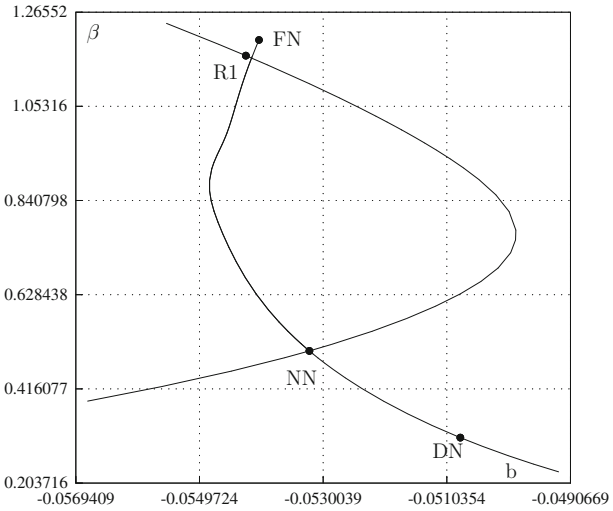

Fig. 21 Bifurcation diagram generated by CONTENT. $\varepsilon = 0.1$. NN stands for Double Neimark–Sacker corresponding with the double Hopf bifurcation in the averaged system, DN stands for Degenerate Neimark–Sacker, corresponding with the generalised Hopf bifurcation in the averaged system. R1 is a 1:1 resonance point corresponding with the Bogdanov–Takens bifurcation and FN is a Fold Neimark–Sacker corresponding with the fold–Hopf bifurcation in the averaged system

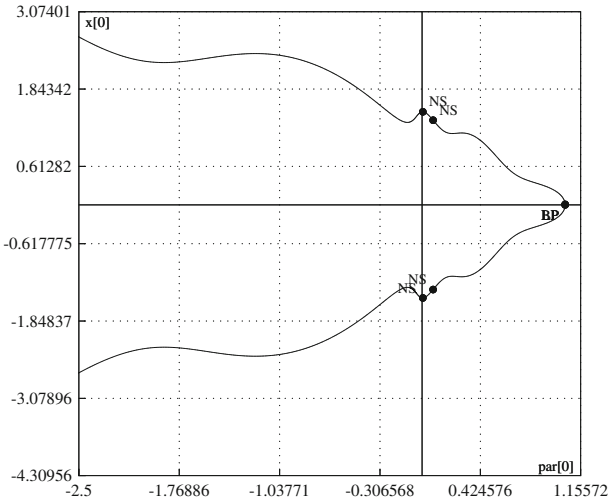

Fig. 22 Time-periodic Poincaré section plotted onto the $b - x_1$ plane obtained with CONTENT by continuation with respect to the parameter b of the unstable equilibrium, corresponding with the 2π-periodic solution; $\varepsilon = 0.05,\ \beta = 1$, NS stands for Neimark–Sacker bifurcation and BP stands for branching point bifurcation. Here the saddle periodic solution collides with the trivial solution in a pitch–fork bifurcation. This branching does also occur in the normal form near the same parameter values but was not shown because it is not relevant to further study of the equilibria

range of existence of the stable and unstable periodic solutions, the normal form predicts surprisingly well the location of the Neimark–Sacker bifurcation involving the stable cycle although the theorems do not guarantee that. Decreasing the parameter ε, for instance taking $\varepsilon = 0.05$, we have found, as expected, topological equivalence between the solutions of the original system and its normal form; see Fig. (22). The persistence of phenomena, in particular periodic solutions, for larger values of the small parameter ε has attracted the attention of several authors; for references see [29, Sect. 10.5].

8 Discussion and Conclusions

1. Using the normal form method of averaging, we were able to detect easily and with very good accuracy bifurcations present in the original system. The mechanical system illustrated by Fig. 1 turns out to have very rich dynamics. In our paper a codimension two bifurcation, the Hopf–Hopf bifurcation plays an important part. The flow around this bifurcation yields stable 3-tori. These tori eventually break-up, leading to strange attractors and ultimately to chaos. Moreover, a new phenomenon was discovered in the bifurcation diagram of the normal form, i.e. the accumulation of period doubling bifurcations in the parameter space yielding a repetitive pattern of the following sequence of codimension two bifurcations: Generalised period doubling (GPD), pitchfork–flip (LPPD), 1:2 resonance (R2), generalized period doubling (GPD), 1:2 resonance (R2) and pitchfork–flip (LPPD). These bifurcations could have been missed easily if one studied the more complex original system directly. It would be interesting to verify whether the period doubling curve of the torus in the original system also exhibits this strange behaviour. To do this, we need to be able to continue tori with respect to parameters. This is however still a very difficult

task to perform numerically. It would be useful to produce a map exhibiting this property and to study it for better understanding the dynamical and geometric meaning of this phenomenon.

2. In the introductory Sect. 1, we have cited the literature on torus bifurcations of maps. It is clear that many of the phenomena found there, can be recognized in our three degrees-of-freedom mechanical system (the Tondl model). The Arnold tongues and resonances that are present are making the dynamics very complex. Still, there emerges a dominant bifurcation picture as many of the resonances give birth to solutions located in thin sets. This picture is reminiscent of Hamiltonian systems near stable equilibrium where the short-periodic solutions, contained in infinite families of invariant tori, dominate the phase-flow, although an infinite set of higher order periodic solutions (of longer period) with associated sets of invariant tori complicate the picture.
3. A study of the system in another possible 1:2:3 resonance, choosing

$$(\omega, \mu, \lambda) = (\sqrt{-0.641}, 2.562, 0.925),$$

did not produce new phenomena and will therefore be omitted here.

4. We gave some attention to the case $m_1 \approx m_3$. In this case the normal form reduces to two coupled oscillators and one uncoupled oscillator. This is still of interest to explore, but because of our focus on phenomena in three degrees of freedom, we have not pursued this.
5. The method of averaging in combination with numerical bifurcation tecniques turns out to be highly efficient to study this type of problems. All the bifurcations detected by the normal form did have their corresponding bifurcations for small values of ε in the original system and were highly accurate.
6. Important open problems are to study the dynamics of the mechanical system described here for other parametric excitation frequencies and also for the basic 1:2:2, 1:2:1 and 1:2:4 resonances.
7. New features of MATCONT to compute normal form coefficients of codimension two bifurcations of limit cycles, see [12], could be exploited.

Acknowledgments Thanks are due to W.L.J. van der Kallen and R.W. Bruggeman for their contribution in the factorisation of the 6-th degree polynomial $P(x)$ (Sect. 3). Comments by J.J. Duistermaat and H.W. Broer are gratefully acknowledged.

Appendix

The Normal Form in x_{ij} Coordinates in the Case $\tilde{\omega} = \omega_0$

The averaged system in the case $\tilde{\omega} = \omega_0$ is as follows

$$\begin{aligned}
x'_{11} &= \varepsilon/8(3x_{11}^3 B_1 - 9x_{11}^2 x_{31} B_1 + 9x_{12}^2 x_{31} B_1 + 36x_{21}^2 x_{31} B_1 - 9x_{22}^2 x_{31} B_1 \\
&\quad +12x_{21}x_{22}x_{32}B_1 - x_{22}Q_{12} + x_{11}(3x_{12}^2 B_1 + 24x_{21}^2 B_1 + 6x_{22}^2 B_1 \\
&\quad +54x_{31}^2 B_1 - 6x_{12}x_{32}B_1 + 6x_{32}^2 B_1 + 4\theta_{11})), \\
x'_{12} &= \varepsilon/8(3x_{12}^3 B_1 + 18x_{11}x_{12}x_{31}B_1 + 36x_{21}x_{22}x_{31}B_1 + 3x_{11}^2(x_{12} - x_{32})B_1 \\
&\quad +3x_{12}^2 x_{32}B_1 - 12x_{21}^2 x_{32}B_1 + 3x_{22}^2 x_{32}B_1 + 2x_{21}Q_{12} + x_{12}(24x_{21}^2 B_1 \\
&\quad +6x_{22}^2 B_1 + 54x_{31}^2 B_1 + 6x_{32}^2 B_1 + 4\theta_{11})),
\end{aligned}$$

$$
\begin{aligned}
x'_{21} &= \varepsilon/24(18x_{11}^2x_{21}B_2 + 18x_{12}^2x_{21}B_2 + 36x_{21}^3B_2 + 9x_{21}x_{22}^2B_2\\
&\quad +162x_{21}x_{31}^2B_2 + 18x_{21}x_{32}^2B_2 + 9x_{11}(6x_{21}x_{31} + x_{22}x_{32})B_2\\
&\quad +3x_{12}(9x_{22}x_{31}B_2 - 6x_{21}x_{32}B_2 - Q_{21}) - x_{32}Q_{23} + 12x_{21}\theta_{22}),\\
x'_{22} &= \varepsilon/8(6x_{11}^2x_{22}B_2 + 6x_{12}^2x_{22}B_2 + 12x_{21}^2x_{22}B_2 + 3x_{22}^3B_2 + 54x_{22}x_{31}^2B_2\\
&\quad +6x_{22}x_{32}^2B_2 + 6x_{12}(6x_{21}x_{31} + x_{22}x_{32})B_2 + 2x_{11}(-9x_{22}x_{31}B_2\\
&\quad +6x_{21}x_{32}B_2 + Q_{21}) + 2x_{31}Q_{23} + 4x_{22}\theta_{22}),\\
x'_{31} &= \varepsilon/24(-(x_{11}^3B_3) + 12x_{12}x_{21}x_{22}B_3 + 3x_{11}(x_{12}^2 + 4x_{21}^2 - x_{22}^2)B_3\\
&\quad +18x_{11}^2x_{31}B_3 + 18x_{12}^2x_{31}B_3 + 72x_{21}^2x_{31}B_3 + 18x_{22}^2x_{31}B_3 + 81x_{31}^3B_3\\
&\quad +9x_{31}x_{32}^2B_3 - x_{22}Q_{32} + 12x_{31}\theta_{33}),\\
x'_{32} &= \varepsilon/8(x_{12}^3B_3 + 12x_{11}x_{21}x_{22}B_3 + 3x_{12}(-4x_{21}^2 + x_{22}^2)B_3 - 3x_{11}^2(x_{12}\\
&\quad -2x_{32})B_3 + 6x_{12}^2x_{32}B_3 + 24x_{21}^2x_{32}B_3 + 6x_{22}^2x_{32}B_3 + 27x_{31}^2x_{32}B_3\\
&\quad +3x_{32}^3B_3 + 2x_{21}Q_{32} + 4x_{32}\theta_{33}).
\end{aligned}
$$

The Normal Form in the x_{ij} Coordinates in the Case $\tilde{\omega} = 2\omega_0$

The averaged system in this case is as follows

$$
\begin{aligned}
x'_{11} &= \varepsilon/24(9x_{11}^3B_1 - 27x_{11}^2x_{31}B_1 + 27x_{12}^2x_{31}B_1 + 108x_{21}^2x_{31}B_1\\
&\quad -27x_{22}^2x_{31}B_1 + 36x_{21}x_{22}x_{32}B_1 + 6x_{12}Q_{11} - 2x_{32}Q_{13} + 3x_{11}(3x_{12}^2B_1\\
&\quad +24x_{21}^2B_1 + 6x_{22}^2B_1 + 54x_{31}^2B_1 - 6x_{12}x_{32}B_1 + 6x_{32}^2B_1 + 4\theta_{11})),\\
x'_{12} &= \varepsilon/8(3x_{12}^3B_1 + 36x_{21}x_{22}x_{31}B_1 + 3x_{11}^2(x_{12} - x_{32})B_1 + 3x_{12}^2x_{32}B_1\\
&\quad -12x_{21}^2x_{32}B_1 + 3x_{22}^2x_{32}B_1 + 2x_{11}(9x_{12}x_{31}B_1 + Q_{11}) + 2x_{31}Q_{13}\\
&\quad +x_{12}(24x_{21}^2B_1 + 6x_{22}^2B_1 + 54x_{31}^2B_1 + 6x_{32}^2B_1 + 4\theta_{11})),\\
x'_{21} &= \varepsilon/8(6x_{11}^2x_{21}B_2 + 6x_{12}^2x_{21}B_2 + 3x_{12}(3x_{22}x_{31} - 2x_{21}x_{32})B_2\\
&\quad +3x_{11}(6x_{21}x_{31} + x_{22}x_{32})B_2 + x_{21}(12x_{21}^2B_2 + 3x_{22}^2B_2 + 54x_{31}^2B_2\\
&\quad +6x_{32}^2B_2 + 4\theta_{22})),\\
x'_{22} &= \varepsilon/8(6x_{11}^2x_{22}B_2 + 6x_{12}^2x_{22}B_2 - 6x_{11}(3x_{22}x_{31} - 2x_{21}x_{32})B_2\\
&\quad +6x_{12}(6x_{21}x_{31} + x_{22}x_{32})B_2 + x_{22}(12x_{21}^2B_2 + 3x_{22}^2B_2 + 54x_{31}^2B_2\\
&\quad +6x_{32}^2B_2 + 4\theta_{22})),\\
x'_{31} &= \varepsilon/24(-(x_{11}^3B_3) + 3x_{11}(x_{12}^2 + 4x_{21}^2 - x_{22}^2)B_3 + 18x_{11}^2x_{31}B_3\\
&\quad +18x_{12}^2x_{31}B_3 + 2x_{12}(6x_{21}x_{22}B_3 - Q_{31}) + 3x_{31}(24x_{21}^2B_3 + 6x_{22}^2B_3\\
&\quad +27x_{31}^2B_3 + 3x_{32}^2B_3 + 4\theta_{33})),\\
x'_{32} &= \varepsilon/8(x_{12}^3B_3 + 3x_{12}(-4x_{21}^2 + x_{22}^2)B_3 - 3x_{11}^2(x_{12} - 2x_{32})B_3\\
&\quad +6x_{12}^2x_{32}B_3 + 2x_{11}(6x_{21}x_{22}B_3 + Q_{31}) + x_{32}(24x_{21}^2B_3 + 6x_{22}^2B_3\\
&\quad +27x_{31}^2B_3 + 3x_{32}^2B_3 + 4\theta_{33})).
\end{aligned}
$$

References

1. Abadi: Nonlinear: dynamics of self-excitation in autoparametric systems. Thesis, Mathematics Institute, Utrecht University, The Netherlands (2003)
2. Afraimovich, V.S., Shil'nikov, L.P.: Invariant two-dimensional tori, their breakdown and stochasticity. Am. Math. Soc. Trans. **149**(2), 201–211 (1991)
3. Arnol'd, V.I.: Dynamical Systems V. Encyclopaedia of Mathematical Sciences. Springer, Berlin (1994)
4. Aronson, D.G., Chory, M.A., Hall, G.R., McGehee, R.P.: Bifurcations from an invariant circle for two-parameter families of maps of the plane: a computer-assisted study. Commun. Math. Phys. **83**, 303–354 (1982)
5. Bajaj, A.K., Tousi, S.: Torus doublings and chaotic amplitude modulations in a two-degree-of-freedom resonantly forced mechanical system. Int. J Non Linear Mech **25**(6), 625–641 (1990)
6. Bakri, T., Verhulst, F.: Bifurcations of quasi-periodic dynamics: torus breakdown. Z. Angew. Math. Phys. (2013). doi:10.1007/s000033-013-0363-8
7. Bakri, T., Nabergoj, R., Tondl, A., Verhulst, F.: Parametric excitation in non-linear dynamics. Int J Non-Linear Mech **39**, 311–329 (2004)
8. Beyn, W.-J., Champneys, A., Doedel, E., Govaerts, W., Kuznetsov, Y.A., Sandstede, B.: Numerical continuation and computation of normal forms. In: Fiedler, B. (ed.) Handbook of Dynamical Systems, pp. 149–219. Elsevier, Amsterdam (2002)
9. Broer, H.W.: Resonance and fractal geometry. Acta Appl Math **120**, 61–86 (2012). doi:10.1007/s10440-012-9670-x
10. Broer, H., Sevryuk, M.B.: KAM theory: quasi-periodicity in dynamical systems. In: Broer, H.W., Hasselblatt, B., Takens, F. (eds.) Handbook of Dynamical Systems, pp. 249–344. Elsevier, Amsterdam (2010)
11. Broer, H., Simó, C., Tatjer, J.C.: Towards global models near homoclinic tangencies of dissipative diffeomorphisms. Nonlinearity **11**, 667–770 (1998)
12. Della Rossa, F., De Witte, V., Govaerts, W., Kuznetsov, Y.A.: Numerical periodic normalization for codim 2 bifurcations of limit cycles. http://arxiv.org/pdf/1111.4445v1.pdf (2011)
13. Dhooge, A., Govaerts, W., Kuznetsov, Y.A.: Matcont: a MATLAB package for numerical bifurcation analysis of ODEs. ACM Trans. Math. Software **29**, 141–164 (2003)
14. Dhooge, A., Govaerts, W., Kuznetsov, Y.A., Meijer, H.G.E., Sautois, B.: New features of the software Matcont for bifurcation analysis of dynamical systems. Math Comput Model Dyn Syst **14**, 145–175 (2008)
15. Doedel, E.J., Paffenroth, R.C., Champneys, A.R., Fairgrieve, T.F., Kuznetsov, Y.A., Sandstede, B., Wang, X.: Auto 2000: continuation and bifurcation software for ordinary differential equations. http://sourceforge.net/projects/auto2000 (2000)
16. Krauskopf, B., Osinga, H.: Growing 1D and quasi-2D unstable manifolds of maps. J Comput Phys **146**, 404–419 (1998)
17. Kuznetsov, Y.A.: Elements of Applied Bifurcation Theory, 2nd edn. Springer, New York (1995)
18. Kuznetsov, Y.A., Levitin, V.V.: Content, a multiplatform environment for analysing dynamical systems. Dynamical Systems Laboratory, Centrum voor Wiskunde en Informatica, Amsterdam, http://www.math.uu.nl/people/kuznet/Content/, (1997)
19. Lin, R., To, C.W.S., Huang, K.L., Lu, Q.S.: Secondary bifurcations of two non-linearly coupled oscillators. J Sound Vib **165**(2), 225–250 (1993)
20. Palis, J., Takens, F.: Hyperbolicity and Sensitive Chaotic Dynamics at Homoclinic Bifurcations. Cambridge University Press, Cambridge (1993)
21. Ruelle, D., Takens, F.: On the nature of turbulence. Comm. Math. Phys. **20**, 167–192 (1971). (23, 241–248 (1971))
22. Ruelle, D.: Differentiable dynamical systems and the problem of turbulence. Bull. AMS **5**, 29–42 (1981)
23. Sanders, J.A., Verhulst, F., Murdock, J.: Averaging Methods in Nonlinear Dynamical Systems. Springer-Verlag, New York (2007)
24. Schilder, F., Osinga, H.M., Vogt, W.: Continuation of quasi-periodic invariant tori. SIAM J. Appl. Dyn. Syst. **4**(3), 459–488 (2005)
25. Shilnikov, A., Shilnikov, L.P., Turaev, D.: On some mathematical topics in classical synchronisation. A tutorial. Int J Bifurcation Chaos **14**(7), 2143–2160 (2004)
26. The program Matcont. http://www.Matcont.ugent.be
27. van Veen, L.: Time scale interaction in low-order climate models. Ph.D. thesis, Mathematics Institute, Utrecht University, The Netherlands (2002)
28. Verhulst, F.: Nonlinear Differential Equations and Dynamical Systems. Springer, Berlin, Heidelberg (2000)

29. Verhulst, F.: Methods and Applications of Singular Perturbations. Boundary Layers and Multiple Timescale Dynamics. Springer-Verlag, New York (2005)
30. Vitolo, R.: Bifurcations of attractors in 3D diffeomorphisms. Ph.D. thesis, University of Groningen, The Netherlands (2003)
31. Vitolo, R., Broer, H.W., Simó, C.: Quasi-periodic bifurcations of invariant circles in low-dimensional dissipative dynamical systems. Regul Chaotic Dyn **16**, 154–184 (2011)